博士学位論文

Study on Epitaxial Growth of Lattice-Matched InGaN through AlN Protection Layer on ZnO Substrate

(ZnO 基板上への AlN 保護層を介した格子整合 InGaN の
エピタキシャル成長に関する研究)

Department of Applied Physics
Graduate School of Engineering
TOHOKU UNIVERSITY
東北大学大学院　工学研究科　応用物理学専攻

Jinyeop YOO
劉　陳燁
B3TD9301

March 28 2019

Abstract

InGaN, an alloy semiconductor of group-III nitride semiconductors, is used as an active layer of highly efficient blue or white light-emitting devices. These devices are fabricated on GaN templates grown on foreign substrates such as sapphire and SiC. There are too large lattice-mismatch between these substrates and GaN to grow high quality InGaN. Moreover, the increase in the mole fraction of InN in InGaN can make InGaN possible to emit the longer-wavelength emission such as green, red, and infrared. ZnO was proposed as a substrate for the growth of InGaN and there was the report on the growth of InGaN on a ZnO substrate in 1989, however, its quality was poor because the poor quality of ZnO itself and the primitive preparation of a ZnO substrate. The growth of InGaN with high quality on a ZnO substrate has been desired for the development of novel InGaN-based devices with high InN mole fraction. All the devices consisting of group-III nitride semiconductors are grown by metalorganic vapor phase epitaxy (MOVPE) because of its several advantages such as the easy composition control, the high uniformity, and the high throughput. There is an issue for the growth of group-III nitride semiconductors on ZnO substrates by MOVPE, because ZnO is chemically unstable to a reducing atmosphere in the MOVPE growth, such as hydrogen as a carrier gas for group-III sources and ammonia as a nitrogen source. This issue has to be solved. In this thesis, the protection layers are formed prior to the MOVPE growth for suppressing the chemical decomposition reaction of ZnO, and the MOVPE growth of an InGaN film on a ZnO substrate is demonstrated.

The average 3.7-mm-thick ZnO bulk crystals were grown by a hydrothermal method together with the joint research company. Screw and edge threading dislocation densities (TDDs) estimated from X-ray rocking curve measurements were 8×10^2 and 4×10^3 cm^{-2}, respectively. These TDDs are much lower than those of GaN epitaxial films on sapphire and SiC substrates. Then 0.5-mm-thick *c*-plane ZnO substrates were fabricated by dicing and chemo-mechanical polishing (CMP). These substrates had rough surfaces with scratches which were caused by the polishing. To improve this surface roughness, the ZnO substrates in an oxidizing atmosphere were annealed at 1150 °C for 4 hours in a box made of ZnO ceramics which could suppress the evaporation of Zn from ZnO. The step-

terrace structure was successfully observed at the surface. Through these processes, ZnO substrates patient for the epitaxial growth could be prepared.

In order to suppress the decomposition of ZnO during the MOVPE growth, a 200-nm-thick single-crystalline AlN film as a protection layer was epitaxially formed on a front surface of ZnO by the pulsed laser deposition (PLD). This PLD enabled the group-III nitride semiconductors to grow without any reactant gas at low temperature. An atomically flat surface was obtained at the growth temperature from 200 to 550 °C. Cracks appeared in the AlN film at higher than 550 °C because of the difference of the thermal expansion coefficient between AlN and ZnO. From an X-ray diffraction (XRD) analysis and an electron backscattered (EBSD) analysis, the PLD-grown AlN film was confirmed to be the c-plane-oriented single crystalline wurtzite structure. This AlN is applicable as a protection layer for the epitaxial growth of InGaN. Both the side wall and the bottom surface of a ZnO substrate were also covered with a SiO_2 film followed by an AlN film. Both films were formed by using the sputtering system. An AlN film resistant to the reducing ambient was necessary because the pits were observed after the annealing at the growth temperature of 800 °C for InGaN for only a SiO_2 film. An AlN film had to be formed on a SiO_2 film because a directly sputtered AlN film on ZnO was partially exfoliated as the origin of hexagonal features formed during annealing at 800 °C. Pits and hexagonal structures disappeared for each thickness of 800 nm of AlN and SiO_2.

Finally, 500-nm-thick InGaN films was MOVPE-grown on a ZnO substrate with the protection layers. For comparison, the MOVPE growth was also performed on both substrates of bare ZnO and sapphire. The source gases for indium and gallium are trimethylindium (TMIn) and triethylgallium (TEGa), respectively. The InN mole fraction was controlled by changing the flow ratio of TMIn and TEGa. The InGaN film on the bare ZnO substrate exfoliated and this ZnO substrate was partially decomposed during the MOVPE growth. On the other hand, the decomposition of the ZnO substrate with the protection layers was drastically suppressed. Structural properties of the $In_{0.18}Ga_{0.82}N$ films were investigated by X-ray rocking curve measurements. $In_{0.18}Ga_{0.82}N$ on the ZnO substrate has narrower full width at half maximum (FWHM) than $In_{0.20}Ga_{0.80}N$, and is confirmed to be almost unstrained from the XRD reciprocal space mapping measurement. It indicates that the $In_{0.18}Ga_{0.82}N$ film can be grown on the ZnO substrate without strain.

The FWHMs of X-ray rocking curves for InGaN 0002 diffraction were 6270 arcsec and 4080 arcsec for the $In_{0.18}Ga_{0.82}N$ films on the ZnO substrate with the protection layer and the sapphire substrate, respectively. The FWHM of the XRC for the InGaN film on the ZnO substrate was wider than that on the sapphire substrate. The degradation of the InGaN crystalline quality might be originated from two reasons. The growth of an InGaN film on a ZnO substrate via an AlN protection layer has two lattice-mismatched hetero interfaces. Both of them have the same lattice mismatch as large as 4%, and the lattice relaxation occurs twice.

In conclusion, even though a ZnO substrate has an instability in a reducing atmosphere, the MOVPE growth of an InGaN film on a ZnO substrate could be enabled by introducing protection layers using the PLD method and the sputtering one. The growth temperature, 800 °C, was 100 – 200 °C higher than previous researches. The results obtained in this thesis increase the availability of substrates and pave the way for new devices fabricated by the MOVPE system.

Table of contents

Acknowledgement

This thesis would never have seen the light without the invaluable help and support of people all the time in Sendai. The following sentences are small expressions to thank them.

First, I would like to appreciate Prof. Jiho Chang in Korea Maritime University for giving a chance to study in Sendai. He has always encouraged me and cared for my situation.

I would like to appreciate Prof. Takashi Matsuoka of Institute for Materials Research (IMR), my supervisor, for sharing his huge experience with me and for leading my work throughout my graduate career. In addition, it could not be possible without the financial support by Prof. Matsuoka that allowed my research to be continued.

I would also like to appreciate Prof. Osamu Kitakami and Prof. Shigefusa F. Chichibu of Institute of Multidisciplinary Research for Advanced Materials for the essential comments which are for the completeness of this thesis.

I would like to thank Prof. Ryuji Katayama of Osaka University for welcoming me as a PLD user, for teaching me everything, and sharing the Japanese culture.

I would also like to thank Senior Assistant Prof. Tomoyuki Tanikawa of IMR for shaping the research project and lead to achieve at close to me.

I would like to thank Assistant Prof. Takashi Hanada and Assistant Prof. Shigeyuki Kuboya of IMR for their insight into the research.

I would like to thank Dr. Takeshi Kimura of SCIOCS for teaching me about all the equipment when he was in Matsuoka laboratory.

I would like to appreciate Emeritus Prof. Tsuguo Fukuda in Fukuda Crystal Laboratory for sharing his technique of the bulk crystal growth.

I would like to thank Ms. Miho Matsuura, Ms. Masako Yukitani, and Ms. Akane Shibata in Matsuoka laboratory for their kind support.

I am grateful my colleagues who served their precious time for me. Assistant Prof. Kanako Shojiki of Mie University, Mr. Takuya Iwabuchi, Mr. Ryohei Nonoda of Mitsubishi Electric, Dr. Prasertsuk Kiattiwut of National Electronics and Computer

Technology Center, Mr. Takashi Aisaka of Toyota Motor Corporation, Mr. Tatsuya Fujita, and Mr. Kazuki Ohnishi. They gave me a help and valuable discussion, and also about Japanese things when they were in Matsuoka laboratory. My thanks go to my dormitory mate, Dr. Hiroyuki Igarashi, who helped me to settle down in Sendai. I thank to Dr. Junghun Choi, Dr. Junho Jung, Dr. Sunjoong Kim, Dr. Sunghoon Kim, Dr. Goonho Park, Dr. Jeonyoung Song, Dr. Yongjun Seo, Dr. Jungsoo Lee, Mr. Sungyong Park, Dr. Choongmoo Shim, Dr. Suenggun Yu, Dr. Jinhyuk Kim, Dr. Seohuen Hong, Dr. Dongsoo Kang, Dr. Soohyun Joo, Mr. Wonyoung Park, Mr. Minkyu Choi, Mr. Sungho Lee, Ms. Chaewon Lee, Mr. Minsik Gong, and Mr. Yunsung Lee in Tohoku University. I was lucky to meet them in Sendai. Also, I am grateful to my friends in Korea.

Finally, I would like to thank my grandmother, my parents, and my sister for their faith and moral support.

List of Figures

List of Tables

Chapter 1. Introduction

In this chapter, as an introduction of this thesis, the background of group-III nitride semiconductors, the necessity of a ZnO substrate, and the key issue of a ZnO substrate in MOVPE, and the purpose and the outlines of this thesis, are described.

1.1 Group-III nitride semiconductors

Group-III nitride semiconductors have been widely used in the application not only the optical devices but also the electronic devices. Their optical transition is direct. Figure 1.1 shows the band-gap energy of group-III nitrides as a function of lattice constants with comparing those of other semiconductors [1,2]. InGaN, an alloy semiconductor of GaN and InN, is used as an active layer in the group-III-nitride-based optical devices. The band-gap energy of InGaN can be changed over a wide range including the visible wavelength region by controlling its alloy composition. The InGaN-based optical devices can cover the whole visible wavelength. Especially for blue light-emitting devices, there is a few candidates of the materials. II-VI semiconductors can also realize the blue light emission. Unfortunately, the devices do not have enough device-lifetime because of the material's instability during the operation [3].

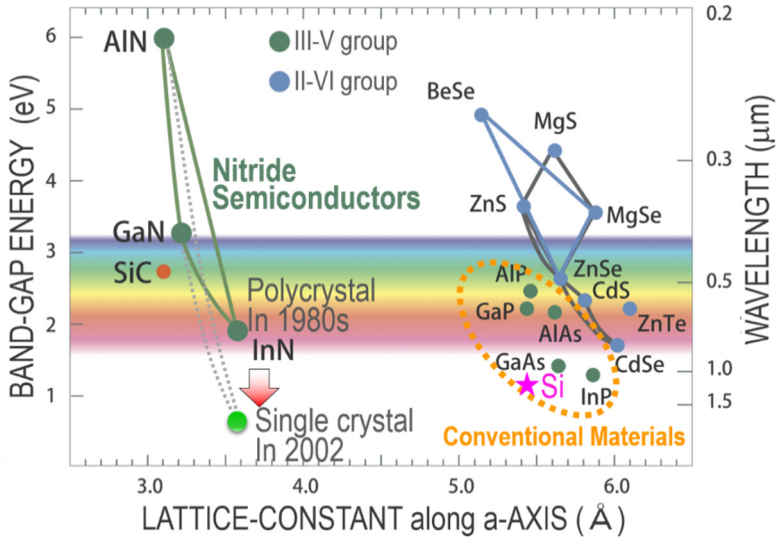

Figure 1.1. Band-gap energy and corresponding wavelength as a function of lattice constant in semiconductors of II-VI and III-V groups.

White light-emitting diodes (LEDs) have been considered as fourth generation light sources. Figure 1.2 shows schematic structures of white LEDs. The most used white LED is composed of an InGaN-based blue LED and a yellow phosphor as shown in Fig. 1.2(a). A yellow phosphor is excited with blue light emitted from a blue LED. Although there is a Stokes energy loss in the conversion from blue to yellow light, the white LED has much higher wall-plug efficiency than other traditional white light sources such as an incandescent light bulb and a fluorescent lamp. In addition, LEDs have very long lifetime more than 10^5 hours. If a white LED is composed of three-colors of LEDs as shown in Fig. 1.2(b) there is no energy loss in their emission process to improve the wall-plug efficiency. By individually controlling the operation power of three LEDs, this white LED can control its color rendering.

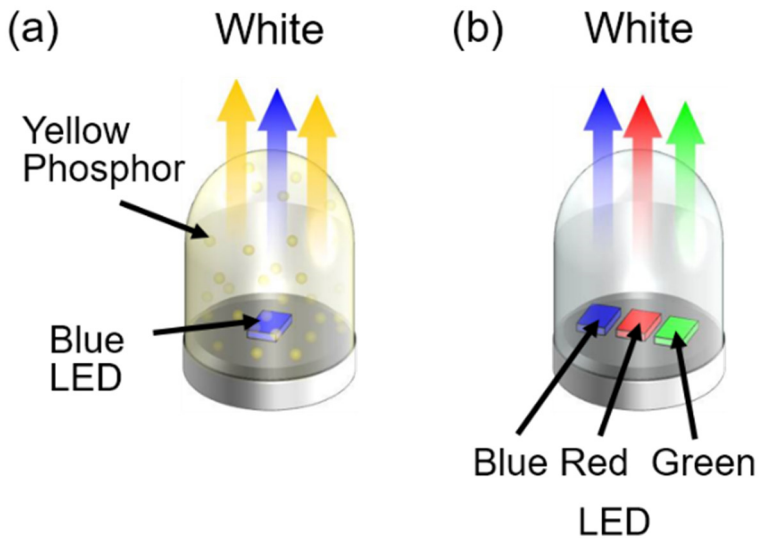

Figure 1.2. Schematic structures of white LEDs composed of (a) blue LED with yellow phosphor and (b) blue, red, and green LEDs.

The white LEDs were commercialized from 1996, and the luminous efficiency was improving year by year. Figure 1.3 shows the trend of luminous efficiency of white light sources. Current commercially-available white LEDs reach their luminous efficiency higher than 180 lm/W. Table 1-1 shows the history and the aspects of the LED penetration ratio to the illumination, and the amount of the energy saving [4]. By replacing light sources from old devices to the white LEDs, the power consumption can be reduced. The

energy saving of lighting in the world in 2025 is expect to reach total power generation in Japan. In other words, LED lighting technology can save energy equivalent to the total electricity consumption in Japan. The LEDs are applied in the wide range fields such as illumination, head lights of vehicles, backlights of liquid crystal display, and so on. All the white LEDs are composed of blue LEDs and phosphors as shown in Fig. 1.2(a).

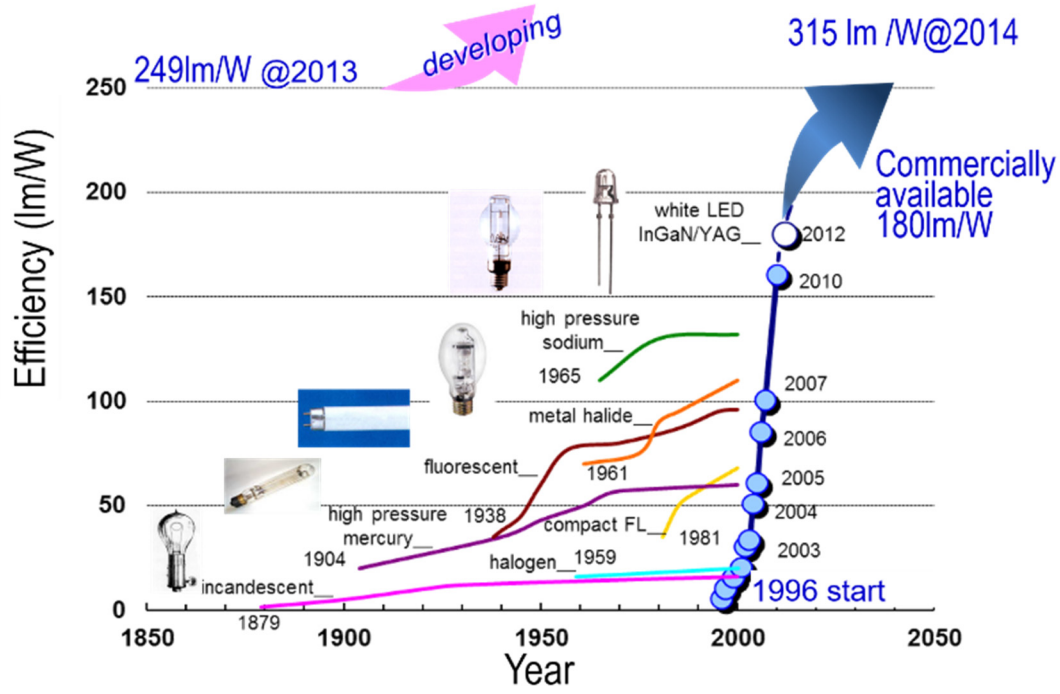

Figure 1.3. Trend of luminous efficiency for white light sources.

Table 1-1. Relations of LED usage and the expected energy saving.

	year	2005	2010	2015	2020	2025
LED Penetration	%	0.05	2	12	30	55
Energy Saving	TWh/yr	2	67	330	720	1,100
Energy Cost Saving	M$/yr	200	6,700	33,000	72,000	110,000
Energy Generating Capacity Savings	GW	0.2	8	38	82	125

In order to improve the luminous efficiency further, the LED, which is composed of

blue, green, and red LEDs as shown in Fig. 1.2(b), is one of the candidates. InGaN can cover the whole visible range by changing its alloy composition. By utilizing InGaN as an emitting layer, red, green, and blue LEDs can be fabricated and a white LED composed of three-colors of LEDs can be fabricated. This white LED has higher efficiency than the white LED composed of a blue LED and yellow phosphor because the Stoke's loss does not occur in its emission process. To realize white LEDs composed of red, green, and blue LEDs, luminous efficiencies of three LEDs should be sufficiently high. However, the external quantum efficiencies (EQEs) of InGaN-based green and red LEDs are still low compared with blue LEDs as shown in Fig. 1.4 [5-8]. One of the reason is the lattice-mismatch in the LED structure of group-III nitride semiconductors as shown in Fig. 1.1. The InGaN active layer is coherently grown on a GaN template. There is a lattice mismatch between these layers. The lattice mismatch results in the generation of large strain in the InGaN active layer. This large strain generates the strong piezoelectric polarization field in the InGaN layer. This field spatially separates electrons and holes in the InGaN active layer, resulting in the reduction of the recombination efficiency. If the thickness of the InGaN active layer exceeds the critical thickness, misfit dislocations are generated at the heterointerface to deteriorate the crystal quality. Therefore a ZnO substrate is introduced for the InGaN growth in this thesis.

Wavelength (nm)	410	450	460	520	560	580	630
Material	$In_xGa_{1-x}N$						
EQE(%)	62	50	84	28	25	13	3

Figure 1.4. EQE of InGaN-based LED as a function of emission wavelength.

1.2 Necessity of ZnO substrate

1.2.1 Substrates for group-III nitride semiconductors growth

Since it is difficult to obtain the own substrate for group-III nitride semiconductors,

the foreign substrates such as sapphire, silicon carbide, and silicon have to be utilized for growth of the group-III nitride semiconductors. Table 1-2 shows the mismatch in lattice constants and thermal expansion coefficients between GaN and the foreign substrates [9-11]. Among them, ZnO has the lattice mismatch as small as 1.9% to GaN. Besides, the crystal structure is the same. Especially, ZnO can be completely lattice matched to $In_{0.18}Ga_{0.82}N$. Therefore the $In_{0.18}Ga_{0.82}N$ film on a ZnO substrate can be expected to have dislocations with the low density.

Table 1-2. Mismatches of lattice constants and thermal expansion coefficients between GaN and foreign substrates.

Substrate	Mismatch (%)	
	Lattice	Thermal Expansion
(0001) Al_2O_3	13.8	-25.5
(0110) Al_2O_3	-1.9, 2.6	9, 62
(0001) 6H-SiC	3.4	25
(101) $NdGaO_3$	1.2	20.6
(001) $LiGaO_2$	0.2, 2.2	19.5, 73.5
(0001) ZnO	-1.9	48

$$\text{Lattice mismatch} \equiv \frac{\text{GaN} - \text{Substrate}}{\text{GaN}}$$

1.2.2 Advantages of ZnO substrate for group-III nitride semiconductors

To fabricate the LEDs, they are fabricated on GaN templates grown on foreign substrates. Sapphire as a substrate has been generally used, however, the group-III nitride films involve high-density threading dislocations due to the lattice mismatch as large as 13.8% between GaN and sapphire. Threading dislocations act as nonradiative centers in an InGaN active layer. In the InGaN/GaN quantum well structure, the electric field is generated with the discontinuity of polarization charges. These polarization charges affect the band diagram as shown in Fig. 1.5 which shows the band diagram of the InGaN/GaN quantum well structure. The electric field is applied to the active layer. It leads the spatial separation of the carriers injected from the outside. This phenomenon is called the quantum-confined Stark effects [12]. The luminous efficiency deteriorates with

increasing the InN mole fraction in InGaN. To obtain the green emission, the InN mole fraction in the InGaN active layer is as high as 30%, then the electric field is very strong to reduce the luminous efficiency.

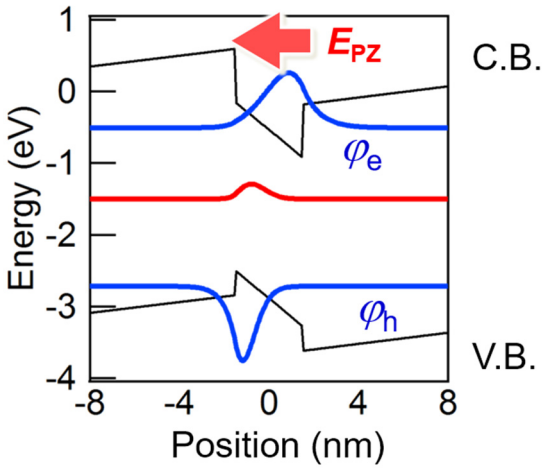

Figure 1.5. Energy-band diagram of InGaN/GaN quantum well and wave functions of electron and hole.

The use of a ZnO substrate can overcome these issues. Schematic structures are shown in Fig. 1.6. When the InN mole fraction in the InGaN film is 18%, the *a*-axis lattice constant of InGaN matches to that of ZnO. Compared with conventional $In_{0.30}Ga_{0.70}N$/GaN on a sapphire substrate, $In_{0.30}Ga_{0.70}N/In_{0.18}Ga_{0.82}N$ on a ZnO substrate can reduce both the threading dislocation density and the polarization field as explained below. First, the in-plane lattice mismatch between $In_{0.18}Ga_{0.82}N$ and ZnO is almost the same. The lattice mismatch between $In_{0.30}Ga_{0.70}N$ and $In_{0.18}Ga_{0.82}N$ is also smaller than that between $In_{0.30}Ga_{0.70}N$ and GaN. In the viewpoint of the lattice-mismatch, the reduction of threading dislocation density can be expected. The polarization field can also be reduced. Therefore the $In_{0.30}Ga_{0.70}N/In_{0.18}Ga_{0.82}N$/ZnO system can be considered to make it possible to obtain longer wavelength optical devices with high luminous efficiency.

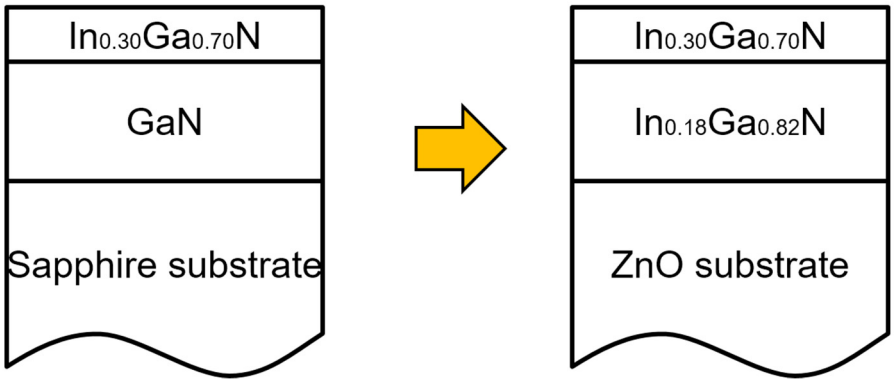

(a) $In_{0.30}Ga_{0.70}N$/GaN/Sapphire (b) $In_{0.30}Ga_{0.70}N$/$In_{0.18}Ga_{0.82}N$/ZnO

Figure 1.6. Schematic structures for the high efficiency of the active layer in the longer wavelength.

1.3 Key issue of ZnO substrate in MOVPE

1.3.1 Introduction of a protection layer

Group-III-nitride devices have been fabricated by using metalorganic vapor phase epitaxy (MOVPE). The key issue for the utilization of ZnO as a substrate is the resistance to the ambient in the MOVPE system because ZnO is chemically unstable to a reducing atmosphere usually used in the MOVPE growth. Reactions in the InGaN growth in the MOVPE system are as follows:

$$In + NH_3 \rightarrow InN + 3/2\,H_2 \quad (1.1)$$

and

$$Ga + NH_3 \rightarrow GaN + 3/2\,H_2. \quad (1.2)$$

During the growth, hydrogen generates from ammonia gas as a nitrogen source. The ZnO substrate is decomposed by hydrogen based on the following reaction,

$$ZnO + H_2 \rightarrow H_2O + Zn. \quad (1.3)$$

H_2 and NH_3 decompose the ZnO substrate. In order to grow an InGaN film on the ZnO substrate without decomposing the ZnO substrate, the introduction of the protection layer for the ZnO substrate is indispensable. In the previous study, a $ZnAl_2O_4$ layer was

introduced as a protection layer in order to suppress the decomposition of ZnO [13]. ZnO films were sputtered on the sapphire substrates. Al was subsequently on the ZnO film by thermal evaporation. Then the sample was annealed at 575 °C for 30 min in the air. The $ZnAl_2O_4$ film was formed by the solid phase reaction between ZnO and Al. GaN films were grown on the ZnO film and the $ZnAl_2O_4$ film by halide vapor phase epitaxy (HVPE). The sample structures are shown in Fig. 1.7. Secondary ion mass spectroscopy (SIMS) profiles are shown in Fig. 1.8. After the GaN growth, Zn and O impurities were diffused to the GaN layer as shown in Fig. 1.8(a). The $ZnAl_2O_4$ film suppressed their diffusion as shown in Fig. 1.8(b).

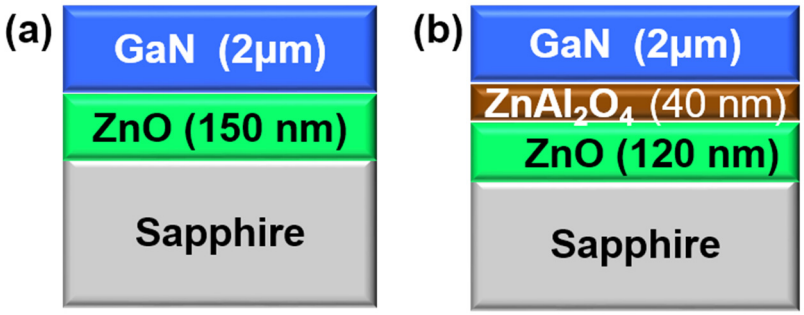

Figure 1.7. Schematic structures of GaN films on ZnO templates (a) without and (b) with $ZnAl_2O_4$ layer.

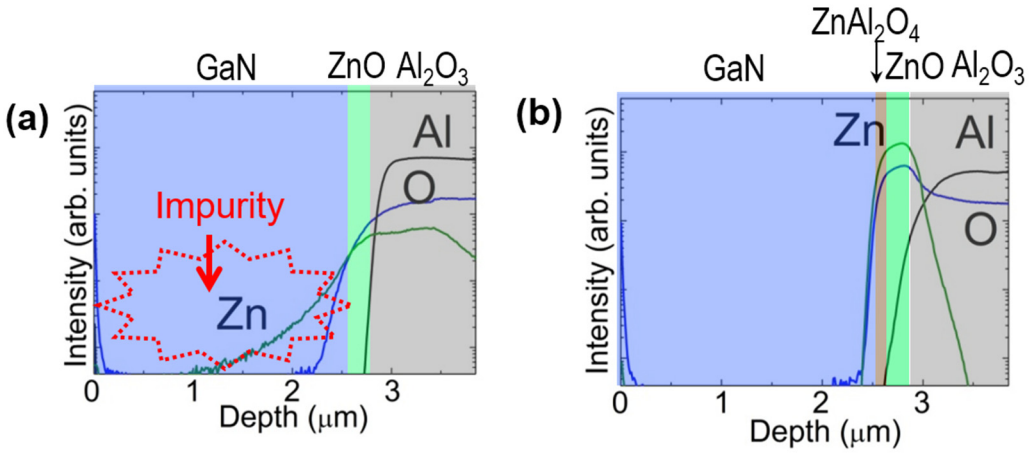

Figure 1.8. SIMS depth profiles of GaN films on ZnO templates (a) without and (b) with $ZnAl_2O_4$ layer.

However the GaN film on the $ZnAl_2O_4$ film was not single-crystalline. This is because the $ZnAl_2O_4$ layer was poly crystalline. Figure 1.9 shows symmetric X-ray

diffraction (XRD) for the sample before the GaN growth. There are two kinds of diffractions from the $ZnAl_2O_4$ layer, indicating that the $ZnAl_2O_4$ layer is polycrystalline. For the epitaxial growth of a single crystalline GaN film, the protection layer should be single-crystalline. There are various methods to obtain single crystal films as shown in Table 1-3. Both the HVPE and MOVPE methods are not appropriate for the growth of a protection layer because they use reactant gases such as HCl, H_2, and NH_3, which decompose ZnO.

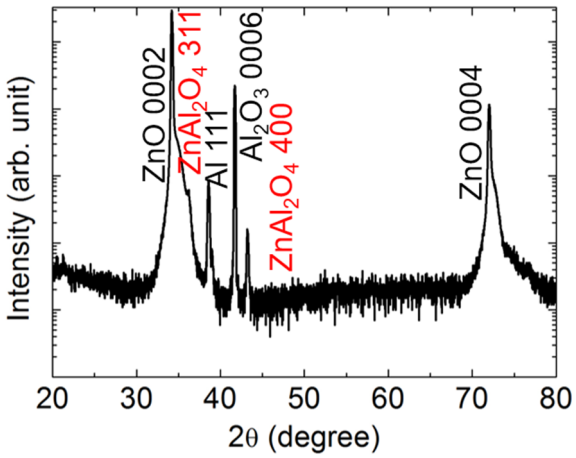

Figure 1.9. 2θ-ω scan of $ZnAl_2O_4$ grown on ZnO/Sapphire.

Table 1-3. Growth methods of single crystalline group-III nitride semiconductors.

Growth method	Characteristics
HVPE	ZnO decomposition with HCl
MOVPE	ZnO decomposition with NH_3 & H_2
MBE	high temperature growth No decomposition of ZnO
PLD	Lower temperature growth No decomposition of ZnO
Sputtering	Low quality

A plasma-assisted molecular beam epitaxy (PA-MBE) method can avoid the ZnO decomposition reaction. PA-MBE uses N_2 plasma as a group-V source instead of NH_3.

Therefore the ZnO decomposition reaction does not occur. However, the high growth temperature more than 700 °C is needed to obtain high crystalline quality because adatoms should migrate to the atomic step edge using thermal energy. The pulsed laser deposition (PLD) and sputtering methods also enable the growth of InGaN films without the ZnO decomposition. Both of them are a kind of the physical deposition methods. Compared with the MBE method, they can grow the films at lower temperature. This is because the source precursors have high kinetic energy at the surface of the substrate. The atoms have sufficient migration length. The atomically flat surface can be obtained [14-16]. In this thesis, PLD method was adopted for the growth of a single crystalline protection layer. The candidate of materials as the protection layer will be discussed in Chapter 3.

1.3.2 Purpose and overview of dissertation

This thesis reports on the growth of a single crystalline InGaN film on a ZnO substrate through the protection layer.

Chapter 1: The group III-nitrides and the ZnO substrates are introduced for the high luminous efficiency for longer wavelength operation.

Chapter 2: The fabrication of the ZnO substrates and annealing of the ZnO substrates are reported.

Chapter 3: The protection layer is grown by PLD on ZnO substrates and the grown films are investigated.

Chapter 4: The back-coat films are deposited by the sputtering method to cover the back side of the ZnO substrates.

Chapter 5: InGaN growth is carried out and discussed.

Chapter 6: Finally, the summary and conclusion is elaborated.

Chapter 2. Fabrication of ZnO Substrate by Hydrothermal Growth

2.1 Introduction

ZnO has been attracted attention for a long time because of its applications ranges in many scientific and industrial areas such as piezoelectric transducers [17], optical waveguides [18], acousto-optic devices [19], conductive gas sensors [20], transparent conductive electrodes [21], varistors [22], and so on. The application for piezoelectric devices is also preferable for ZnO because of its high piezoelectric responsibility [23]. By utilizing the wide band-gap energy and the conductivity of ZnO-related compounds, the materials can be used as the transparent conductive films. In order to realize these devices, it is important to develop the growth technology of ZnO thin films with high quality. For the growth of a ZnO bulk crystal, four techniques such as the hydrothermal growth from aqueous alkaline solutions or solvothermal one [24-26], melt-growth [27], physical and chemical vapor transport, and solution or flux growth [28,29] have been developed.

In order to obtain an epitaxial film with high crystalline quality, the crystalline quality of a substrate should sufficiently be high. In addition, the surface preparation is necessary prior to the procedure of the epitaxial growth. In this study, the fabrication process of ZnO substrates is investigated.

2.2 Hydrothermal growth

The hydrothermal method is defined as a synthesis method for growing single crystals from the chemical reaction of an aqueous solution in an autoclave at high temperature and pressure. The essence of the hydrothermal method is to create the conditions that make supersaturated solution, which dissolves source precursors. The source precursors are not dissolved in the solution at low temperature and low pressure. In an elevated temperature and pressure, the source precursors are dissolved in the solution. Schematic structure of an autoclave is shown in Fig. 2.2.

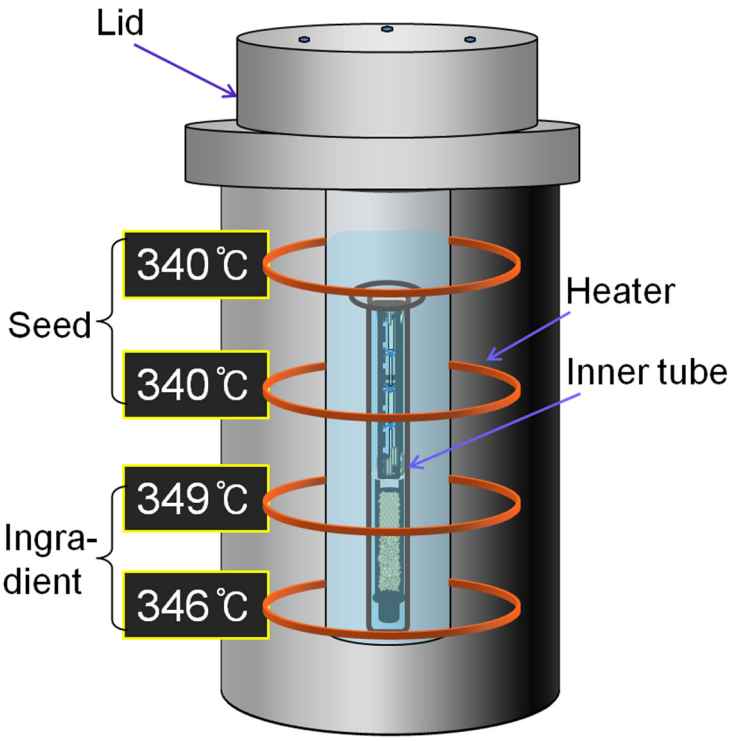

Figure 2.1. Schematic structure of autoclave for growth of ZnO bulk crystal.

An autoclave is composed of an inner tube and four heaters. An inner tube consists of compounds such as Pt, Ag, and Ti, which do not react with solvents. A ZnO seed is put in the inner tube. A mixed solution of KOH and LiOH is used as the mineralizer. The mole ratio of KOH and LiOH are 3:1. This mole ratio can avoid the anisotropic growth rate between *m*-axis and *c*-axis of the ZnO crystal as shown in Fig. 2.2(a). It was reported by Sakagami *et al.* and they controlled the growth rate between *m*-axis and *c*-axis of ZnO crystal when the mole ratio of KOH and LiOH are 3:1 as shown in Fig. 2.2(b) [30]. Deionized water was mixed into the mineralizer. The ratio of water and the mineralizer is 0.48:0.52. It is put into the autoclave. The heating area can be separated two parts: the seed region and the growth region. The seed region is located above the growth region. The temperature of each region is controlled individually by different heaters. During the growth, the seed region was maintained at 340 °C. The temperature of the growth region was maintained between 346 °C and 349 °C. The growth region has temperature gradient as shown in Fig. 2.2. The difference of the temperature between the seed region and the

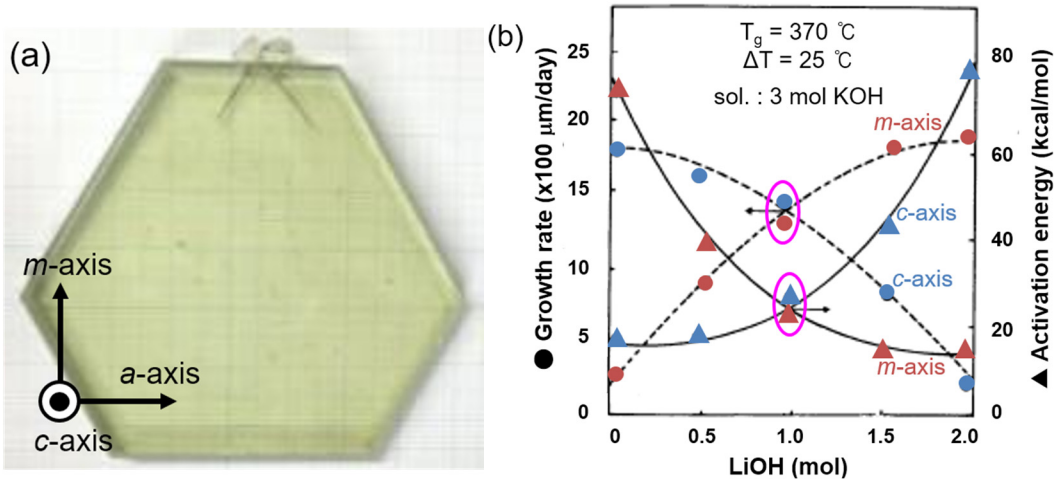

Figure 2.2. (a) Photograph of ZnO crystal and (b) growth rate and activation energy as a function of LiOH mole ratio.

growth one is approximately 9 °C. This temperature gradient induces the reaction of the ingredient melting and the precipitation at the seeds. The temperature was maintained at 65.7 MPa for three weeks to proceed the growth of ZnO crystals.

There are the advantages of the hydrothermal technique in the relatively low growth temperature at the solid/liquid interface, an easily scalable technique, and the potential to reduce the impurities. However, the presence of solution elements such as lithium, sodium or potassium including LiOH, NaOH, or KOH as mineralizers can result in their incorporation. The growth rate of this method is as slow as about 10 mm/day. The growth rate was limited because OH and H_2O tend to be incorporated into the crystal at higher growth rate. General aspects of the hydrothermal growth technique applied to ZnO can be found in the literature [31-33].

In this study, the ZnO bulk growth is demonstrated using the hydrothermal method. A growth condition is shown in Table 2-1. About 1-mm-thick ZnO plates were used as seed crystals. First, the seed crystals were etched in KOH at 60 °C for 90 min in order to remove the impurity contamination existed near the surface. Then they were introduced into the reactor.

Table 2-1. Growth conditions of ZnO crystal by hydrothermal method.

Temperature (°C)	340 - 350
Discrepancy of temperature (°C)	5 – 10
Duration (week)	3
Pressure (MPa)	65.7
Mineralizer	KOH, LiOH
Material	ZnO
Inner tube size (Φ)	70

Figure 2.3(a) shows a photograph of ZnO crystals hanging on the frames just after the growth for approximately 16 days. Their average thickness was 3.7 mm. The growth rate was 0.227 mm/day. The slow growth rate is necessary to reduce unintentional impurity incorporation. 0.5-mm-thick ZnO substrates were fabricated from the bulk ZnO crystals with dicing and CMP. A photograph of the fabricated ZnO substrate is shown in Fig. 2.3 (b).

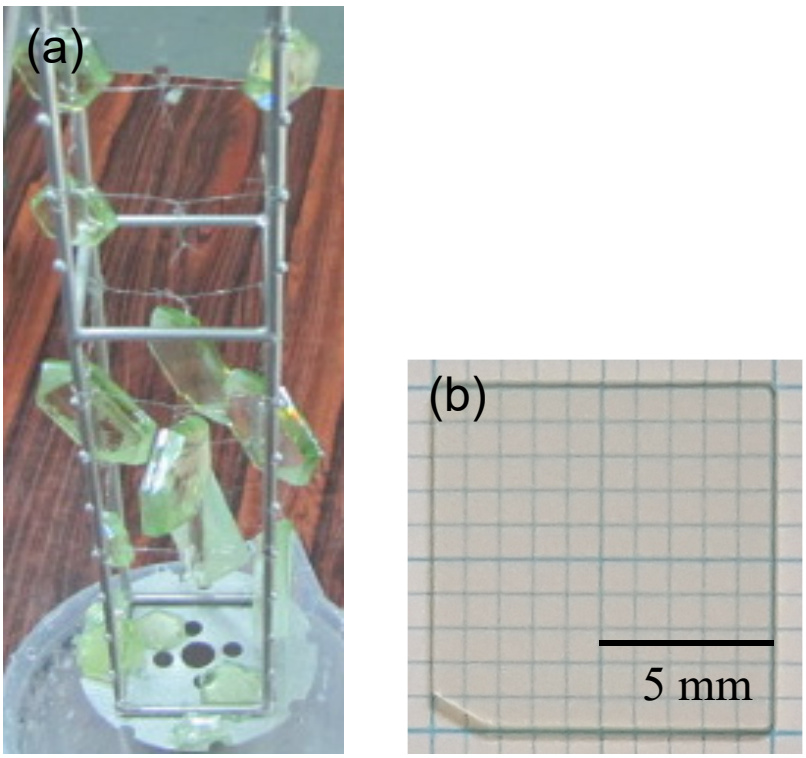

Figure 2.3. Photographs of (a) as-grown ZnO crystals by hydrothermal method in Fukuda crystal laboratory and (b) 10 × 10 mm^2 ZnO substrate.

The crystalline quality of this ZnO substrate was investigated by X-ray rocking curve (XRC) measurements. The full width at half maximum (FWHMs) of XRC for 0002 and $10\bar{1}1$ diffractions were 21.4 and 45.5 arcsec, respectively. These values are comparable with commercially available ZnO substrates as shown in Table 2-2.

Table 2-2. Comparison of FWHMs of XRC for 0002 and $10\bar{1}1$ diffractions of ZnO substrate fabricated in this study and commercially available one.

Diffraction plane	FWHM (arcsec)	
	This study	Commercialized
0002	21.4	15.5
$10\bar{1}1$	45.5	90.6
$10\bar{1}0$	42.2	–

2.3 Surface treatment by annealing

The fabricated ZnO substrates have surface damage such as scratches on a surface during the CMP process. This surface damage interrupt the epitaxial growth. Therefore, it is necessary to improve the surface morphology through the surface re-arrangement and the thermal annealing is carried out. In the case of ZnO substrates, they should be annealed in an oxygen atmosphere because Zn is evaporated at high temperature [34,35]. There is the other way, putting in a ZnO ceramic, to obtain an atomically flat surface [36]. Kobayashi *et al.* annealed the ZnO substrates in a box made of ZnO ceramics, in order to prepare the epi-ready surface for the subsequent growth of an InGaN film by the pulsed sputtering method [36]. They prevented Zn atoms in a ZnO substrate from evaporating.

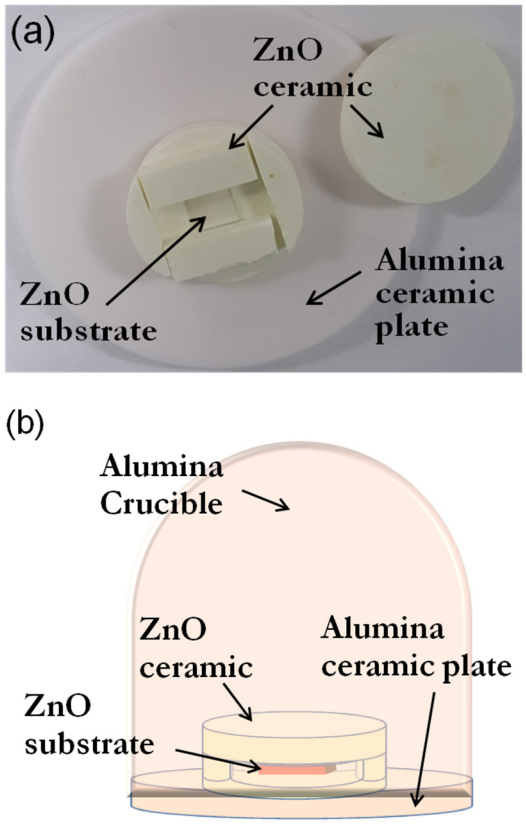

Figure 2.4. (a) Photograph of alumina and ZnO ceramics and (b) schematic of assembly.

A Zn-polar ZnO substrate was cleaned by dipping in ethanol for 5 minutes with an ultrasonic. Then, the ZnO substrate was put on a ZnO ceramic disk. As shown in Fig. 2.4(a), the ZnO substrate was surrounded with the ZnO ceramics. The ZnO ceramic including the ZnO substrate was covered with the alumina crucible to avoid the contamination from the impurity attaching to the inside of a furnace. Figure 2.4(b) shows the illustration which explains how to anneal the ZnO substrate. This assembly was introduced in an electric furnace. The ZnO substrates were annealed at 900 - 1200 °C for 4 hours in an air atmosphere without any gas flow. The surface morphology and the crystal quality of the ZnO substrates were evaluated with an atomic force microscopy (AFM) and an XRC measurement, respectively. The surface morphology of each sample annealed at various temperatures was observed by AFM. Figure 2.5 shows AFM images of ZnO substrates before (Fig. 2.5(a)) and after (Figs. 2.5(b) – 2.5(f)) annealing. The scratches remained on the surface at the annealing temperature lower than 1000 °C. For the samples annealed at 1100 – 1200 °C, the scratches disappeared, and the step and

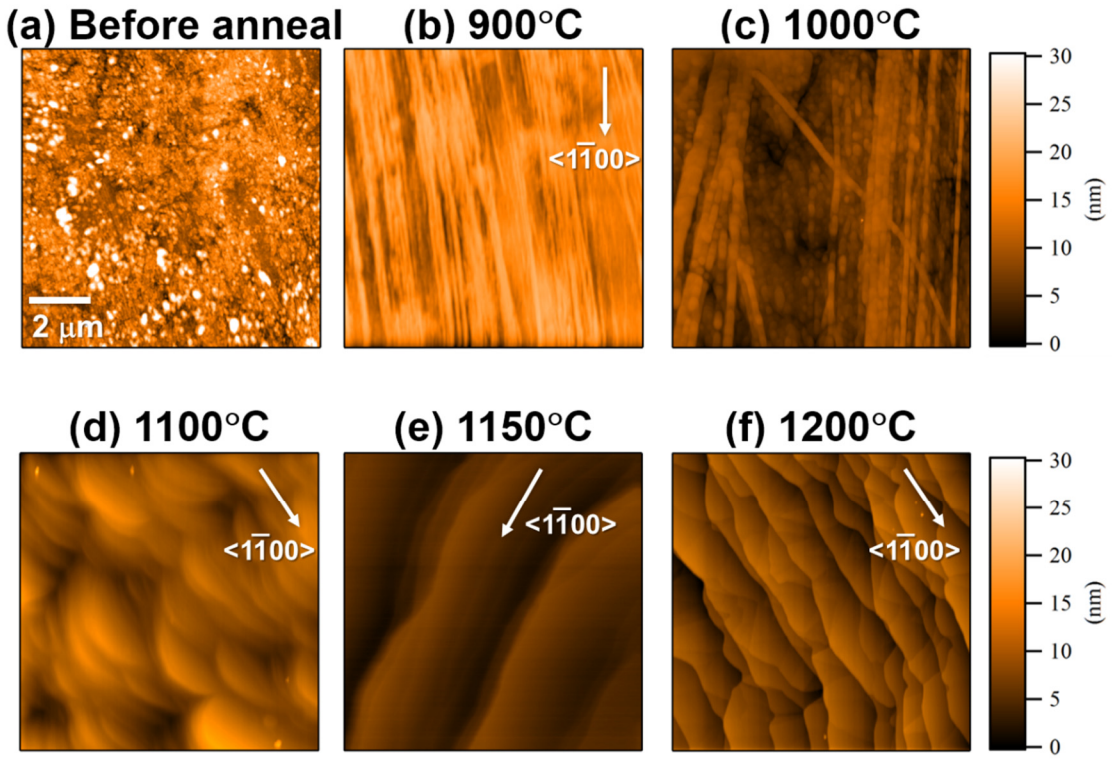

Figure 2.5. AFM images of the ZnO substrates (a) before and (b-f) after annealing.

terrace structure appeared. Root means square (RMS) roughness is shown in Fig. 2.6. The surface roughness was improved by annealing. The RMS roughness values are 5.2 nm for Fig. 2.6(a), 2.9 nm for Fig. 2.6(b), 2.2 nm for Fig. 2.6(c), 2.0 nm for Fig. 2.6(d), 1.1 nm for Fig. 2.6(e), and 1.7 nm for Fig. 2.6(f). At the annealing temperature of 1150 °C, the atomic step and terrace structure appeared. The average step height was 1.13 nm, which was approximately equal to twice *c*-axis lattice constant of ZnO (0.5206 nm). It implies that the atomic re-arrangement at the surface was achieved by annealing.

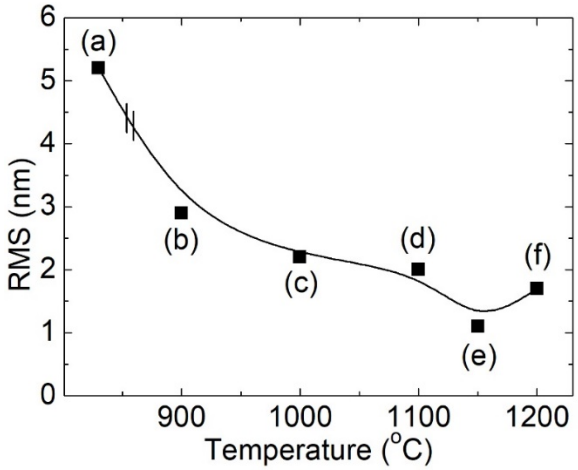

Figure 2.6. RMS of the ZnO substrates (a) before and (b-f) after annealing.

The crystalline quality of the ZnO substrates annealed were investigated by XRC measurements. Table 2-3 shows the FWHMs of the XRCs for the ZnO substrates before and after annealing at 1150 °C. FWHMs of both symmetric and asymmetric diffractions decreased by thermal annealing. It indicates the scratched surface region including the area with poor crystalline quality was removed by annealing. Therefore it can be concluded that the fabricated ZnO substrate has enough crystalline quality applicable for the growth of group-III nitride semiconductors, because these FWHMs are much narrower than those of typical hetero epitaxially-grown GaN films.

Table 2-3. XRC FWHMs of 0002 and $10\bar{1}1$ before and after annealing of a ZnO substrate at 1150 °C.

	FWHM (arcsec)	
	0002	$10\bar{1}1$
Before annealing	21.4	45.5
After Annealing	20.4	29.4

The relation between annealing and the optical properties of ZnO substrates was investigated. Figure 2.7 shows photoluminescence (PL) spectra of (a) the as-polished and

(b) the annealed ZnO substrates at 1150 °C for 4 hours. The dominant PL emission of all the samples was the near-band edge emission. The deep level emission (DLE) was also observed around 539 nm. The intensity of DLE was different for each sample. The increase of DLE is attributed to the oxygen vacancies. They are generated by the insufficient partial pressure of oxygen during annealing [38]. Whereas, both polarity of the ZnO substrates showed higher intensity of DLE than as-polished ZnO substrates. This situation can be observed independently on the annealing temperature.

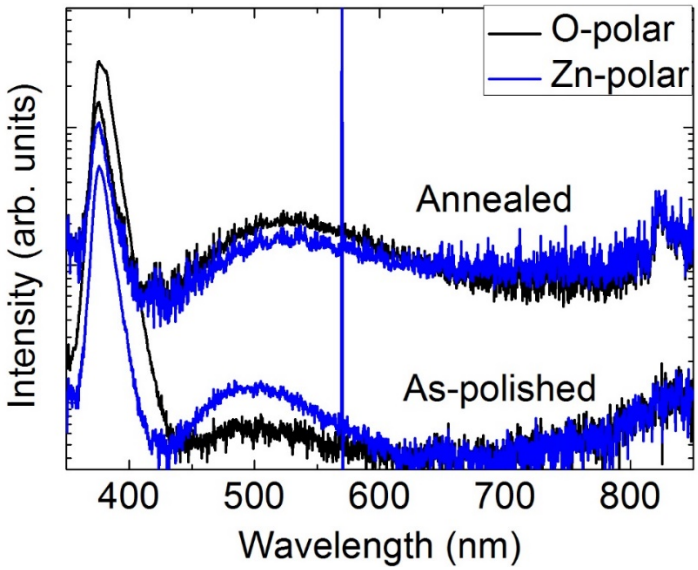

Figure 2.7. Photoluminescence spectra of (a) as-polished and (b) annealed ZnO substrates measured at room temperature.

2.4 Summary

ZnO crystals were successfully grown by the hydrothermal method. *c*-plane ZnO substrates were fabricated through dicing, CMP, and annealing processes. After the CMP process, scratches appeared at the surface of the ZnO substrate. By annealing the ZnO substrates in the ZnO ceramics box, these scratches disappeared. The annealing process made the surface flat. The proper annealing temperature for obtaining a smooth surface morphology with an atomic step and terrace structure was 1150 °C. Its RMS roughness was as low as 1.13 nm. The ZnO substrate with an almost atomically flat surface of can be fabricated. The FWHMs of XRCs for the ZnO substrate were improved by annealing. They are comparable with those of the commercial ZnO substrates. The FWHMs are

much narrower than typical hetero epitaxial GaN films. Therefore, the ZnO substrates are concluded to have enough crystalline quality for the use of the epitaxial growth of group-III nitride semiconductors. In the viewpoint of the surface morphology and the crystalline quality evaluated by the X-ray diffraction, it can be concluded that a ZnO substrate for the epitaxial growth of group-III nitride semiconductors can be obtained.

Chapter 3. Epitaxial growth of AlN protection layer by pulsed laser deposition

3.1 Introduction

3.1.1 Pulsed laser deposition

Most of the group-III nitride semiconductors are grown by MOVPE because it has already proved very practical for commercially realized device fabrication. However, the pulsed laser deposition (PLD) method has several attractions for the growth of group-III nitride semiconductors such as (i) the selective doping of atoms, (ii) a variable stoichiometric transfer from the target material [39], and (iii) the reduction of the interface reactions [40,41], which was previously thought to be obtainable in molecular beam epitaxy methods [42,43] and is important for optoelectronic device fabrication. Indeed, (iii) is a significant issue since the numerous interface reactions between the ZnO substrate and the grown film have been reported [44-47].

PLD is well known as a physical vapor deposition (PVD) method, carried out in an ultra-high vacuum (UHV) system. In PLD, shown schematically in Fig. 3.1, a pulsed laser is irradiated on a target of the material to be desorbed. For sufficiently high laser energy density, each laser pulse ablates the target material and produces plasma of the target. This plasma state is called plume. The ablated target materials are desorbed from the target in a highly forward directed plume. These desorbed target materials adsorbed at the surface of the substrate. Through the migration process, they crystallize. The ablation plume provides the material flux for the film growth. PLD has proven remarkably effective at yielding epitaxial films [48-51]. PLD enables the AlN growth at lower temperature because it employs the high energy laser to promote the long migration of the energetic ablated particles on the growing surface. Thus, it is possible to grow a similar quality films, that can be obtain by MOVPE at around 1100 °C, at low temperature by PLD. The in-situ observation of the surface state can be implemented by reflection high-energy electron diffraction (RHEED). The discrepancy between the thermodynamic energy and the scattered particle energy, which correspond to the MOVPE and PLD methods, is calculated by (3.1) and (3.2), respectively,

$$E = kT \cong 118.4 \text{ meV} \quad (3.1)$$

and

$$E = hf \cong 5009.5 \text{ meV}. \quad (3.2)$$

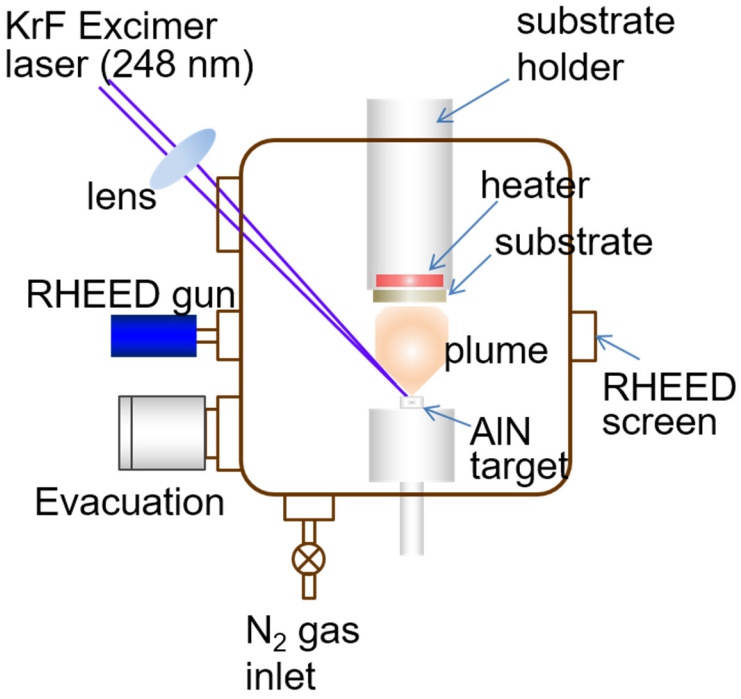

Figure 3.1. Illustration of PLD apparatus.

3.1.2 Targets for AlN growth

There are two alternatives in PLD growing group-III nitride semiconductors: the group-III metal and nitride targets. Group-III metal targets can be commercially obtained and their purity is as high as 99.999%. Although there is an advantage of the comparatively high target purity, a problem was reported on a metal target in a vacuum chamber of PLD. Toth *et al*. have studied the surface dynamics of ablated metal targets, which have a low melting point. They observed that the rippled structure developed on the surface of the target [52]. Besides, they noted that a distinct liquid droplets occurred when ablating Bi targets. In and Ga metals have low melting temperatures. Therefore, the similar problem of laser-ablated molten metal target surfaces is probable. Therefore, the pressed pellets prepared from nitride powders with 99.9% purity have been regarded as the better choice than the group-III metal targets. Preparation of ceramic targets for laser ablation involves grinding and pressing of the powders followed by calcination to remove

volatile impurities such as group-III oxides [53]. To obtain a high density and mechanically robust target, this process is implemented by sintering of the pressed pellets [54], and is sometimes reiterated [55]. However, thermally sintered GaN or InN targets are not commercially available until now. So the AlN is employed as a protection layer for the metal organic vapor phase epitaxy of InGaN films on ZnO substrates.

3.1.3 Purpose

In this chapter, PLD growth of an AlN epitaxial layer at low temperature as a protection layer was performed on a ZnO substrate to realize the MOVPE growth of InGaN films on the ZnO substrate without decomposition reaction. This is because AlN is resistant to the harsh MOVPE environment. The crystal quality, strain, and morphology of the grown AlN layer was investigated.

3.2 Experiment

The conditions for the AlN growth on MOVPE-grown Ga-polar (0001) GaN on sapphire instead of bulk ZnO substrates were optimized as the first step toward the MOVPE growth of group-III nitride semiconductors on ZnO substrates. The sapphire substrates were treated in acetone, methanol, and deionized water under ultrasonic vibration. For the preparation of Ga-polar GaN templates, GaN films were grown on (0001) sapphire substrates with two steps: a low temperature GaN buffer layer growth followed by a GaN layer growth. The low temperature GaN buffer layer was grown at 550 ºC with a V/III ratio of 3620. Then a GaN layer was grown at 1060 ºC with a V/III ratio of 3960. Each step was optimized for the Ga-polar GaN growth. Approximately 200-nm-thick AlN films were grown on the GaN/sapphire templates at 200 ºC, 350 ºC, and 550 ºC by PLD. An AlN target with 99.9% purity was used. After the sample was introduced into the reactor, the background pressure was reduced to 2×10^{-7} Pa. Then N_2 was put into the reactor. Under N_2 ambient at 3.0 Pa, an excimer laser (200 mJ, 10 Hz) with KrF radiation with an emission wavelength of 248 nm was irradiated to ablate the AlN target. The energy of the laser was 200 mJ/pulse and the repetition rate was 10 Hz.

The AlN films were also grown on ZnO substrates. The conditions were maintained as same as the growth conditions of the AlN film on the GaN template and the growth

temperatures were varied between 350 °C and 550 °C.

The surface morphology and structural properties were characterized by RHEED, XRD, electron backscatter diffraction (EBSD) analyses, optical microscopy, atomic force microscope (AFM), and scanning electron microscope (SEM).

3.3 Comparison of AlN growth on GaN template and ZnO substrate

3.3.1 Single crystal AlN growth on GaN template

The AlN films were grown on the Ga-polar GaN templates at growth temperatures of 200 ºC, 350 ºC, and 550 ºC and reactor pressures of 1.0 Pa, 3.0 Pa, and 5.0 Pa. The XRD 2θ-ω symmetric scan around the GaN 0002 diffraction is shown in Fig. 3.2. The AlN 0002 diffraction was observed from all the samples except the samples grown at 200 °C and 1 Pa and 5 Pa. The appearance of the AlN 0002 diffraction indicates that the AlN film is oriented in the (0001) plane. The diffraction peak position of unstrained AlN is 36.04°, which is indicated in Fig. 3.2 by the dashed line. For the sample grown at 1 Pa, the AlN 0002 diffraction peak was located at 35.75°, which is smaller than that of unstrained AlN. This shift of diffraction peak position corresponds to an increase of interplanar spacing of *c*/2 by 1.9 – 3.1% from unstrained AlN. At higher pressure of 3.0 Pa, as shown in Fig. 3.2(b), the AlN 0002 diffraction peaks (pink arrows) corresponded to the interplanar spacings 0.69%, 0.27%, and 0.04% larger than the *c*/2 of unstrained AlN. At 350 °C, the AlN 0002 diffraction had a shoulder corresponding to the *c*/2 of unstrained AlN. For the sample grown at 200 °C and 5 Pa, AlN related diffraction peaks were not observed.

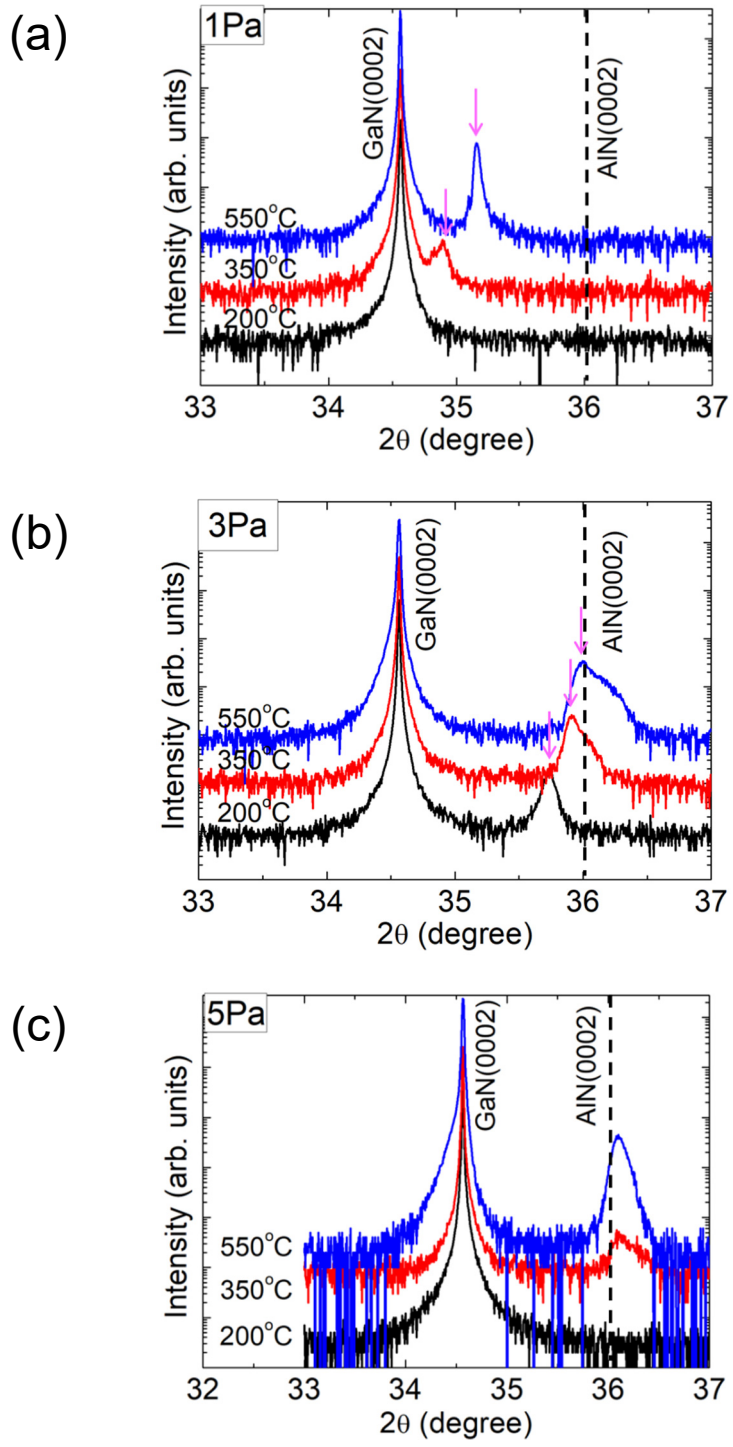

Figure 3.2. XRD 2θ-ω scan results of AlN films on GaN templates grown at (a) 1.0 Pa, (b) 3.0 Pa, and (c) 5.0 Pa.

The AlN 0002 diffraction peaks grown at 350 ºC and 550 ºC appeared at 36.10° and 36.08°, which corresponds to 0.23% and 0.19% smaller than the *c*/2 of bulk AlN. The strain of the AlN films is due to the mismatch of thermal expansion coefficient (TEC) between the AlN film and the sapphire substrate. The TEC of AlN is slightly smaller than that of sapphire. The interplanar spacing of the AlN film is shortened by the mismatch of TECs. Therefore, if only the strain is caused by the mismatch in the TEC, the 0002 interplanar spacing of the AlN film must be slightly smaller than that of the bulk one. It is in contrast to the experimental results for the samples grown at 1.0 Pa and 3.0 Pa. The diffraction peak shift observed for the samples grown at these low N_2 pressures might be caused by the zincblende-like stackings [56], because the interplanar spacing of the zincblende AlN (111) layer is 1.5% larger than that of the wurtzite AlN (0001) layer. When the interplanar spacing is larger than the wurtzite (0001) layer, the diffraction of the AlN film appears at the smaller angle.

In order to confirm the crystal structure of AlN in detail, EBSD was measured. The result for the AlN film grown at 3.0 Pa and 350 °C was shown as a typical result among the measured samples which have same results. The phase image and Kikuchi pattern of AlN films are shown in Figs. 3.3(a) and 3.3(b), respectively. In the phase image, the red and green colors correspond to the wurtzite and zincblende structures, respectively. The Kikuchi pattern of the AlN films, which had six-fold rotational symmetry around the surface-normal zone axis. It indicate that of the AlN films had hexagonal structure. It is concluded that the AlN films on the GaN templates grown by PLD are *c*-oriented wurtzite crystals, at least in the range of the escape depth of EBSD electrons (a few tens of nanometers). It has been reported that the compressive XRD peak shift of AlN was observed when the sputtering pressure was low during the sputtering growth [57,58], which is similar with PLD growth. The diffraction peak position of the AlN bulk exists between the diffraction peaks of the AlN films grown at 3.0 Pa and 5.0 Pa at 350 °C. Consequently, the AlN growth can be expected to optimize at about 4.0 Pa and 350 °C according to the diffraction peak position of the AlN 0002 diffraction.

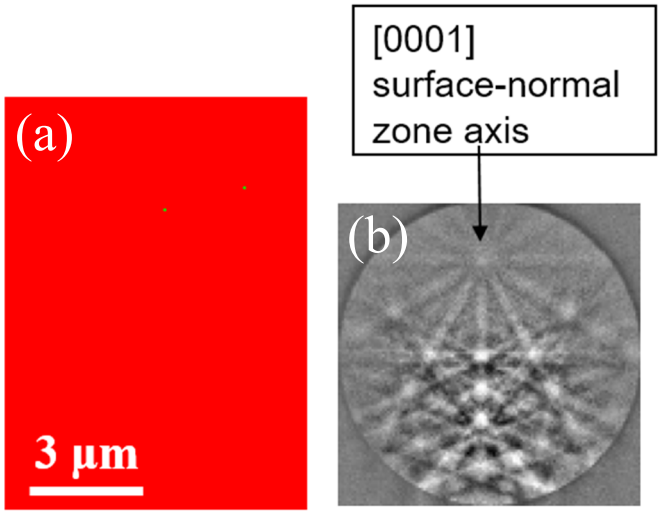

Figure 3.3. (a) Phase image (red: wurtzite, green: zincblende) and (b) Kikuchi pattern of AlN film on Ga-polar GaN template grown by PLD at 3.0 Pa and 350 ºC.

In order to investigate the surface morphology of the AlN films, AFM measurement was carried out. The samples grown at 3.0 Pa and 5.0 Pa were compared because they had small strain in the AlN films. 5×5 µm^2 AFM images of the AlN films grown at the pressure of 3.0 Pa and at 200 °C, 350 °C, and 550 °C are shown in Figs. 3.4(a), 3.4(b), and 3.4(c), respectively. When the growth temperatures were 200 °C and 350 °C, a step-terrace structure appeared without any cracks. As shown in Fig. 3.4(c), a crack was observed on the AlN surface grown at 550 °C. The root mean square (RMS) values, indicating numerical criterion of a surface roughness, were 3.0 nm, 2.6 nm, 2.0 nm, respectively. The higher temperature tends to result in a smoother surface, but the cracks appeared due to the difference of TECs between AlN and GaN multiplied by the temperature difference between the highest growth temperature 550 °C and the room temperature. The cracking mechanism between the AlN film and the GaN template is explained in Fig. 3.6.

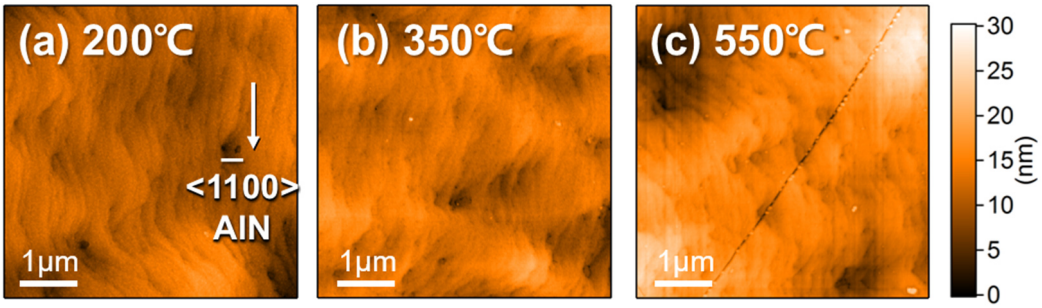

Figure 3.4. 5 × 5 μm^2 AFM images of AlN films on GaN templates grown at (a) 200 °C, (b) 350 °C, and (c) 550 °C in 3.0 Pa.

Figures 3.5(a), 3.5(b), and 3.5(c) show the surface morphologies of AlN films grown at the pressure of 5.0 Pa and at the temperatures of 200 °C, 350 °C, and 550 °C, respectively. They have comparatively worse roughness than the AlN films grown at 3.0 Pa. The RMS roughness values of AlN films grown at 200 °C, 350 °C, and 550 °C were 5.2 nm, 5.8 nm, 2.7 nm, respectively. Figures 3.5(a) and 3.5(b) are not proper surfaces for the further InGaN epitaxial growth because these surfaces are too rough. Figure 3.5(c) shows the numerous cracks than AlN films grown at 3.0 Pa at the same temperature. It implies that the tensile stress, which is confirmed by the XRD 2θ-ω scan, augmented the cracks of the AlN films.

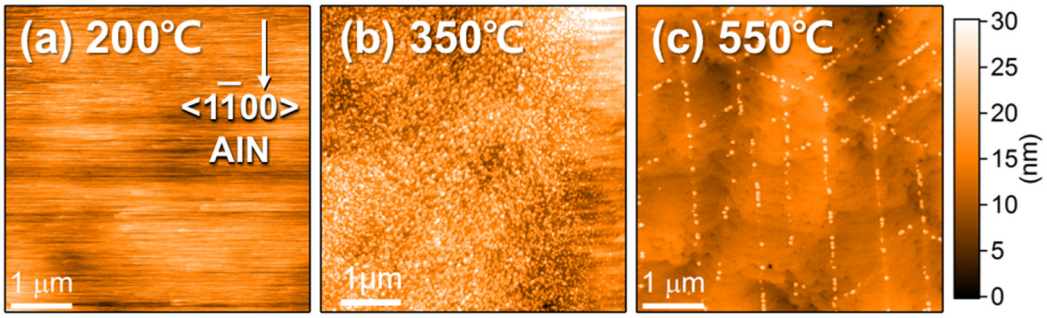

Figure 3.5. 5 × 5 μm^2 AFM images of AlN films on GaN templates grown at (a) 200 °C, (b) 350 °C, (c) 550 °C and 5.0 Pa.

Figure 3.6 shows the cracking mechanism of AlN films grown at 550 °C. When the AlN films were grown on the GaN templates, a dominantly thick sapphire substrate is

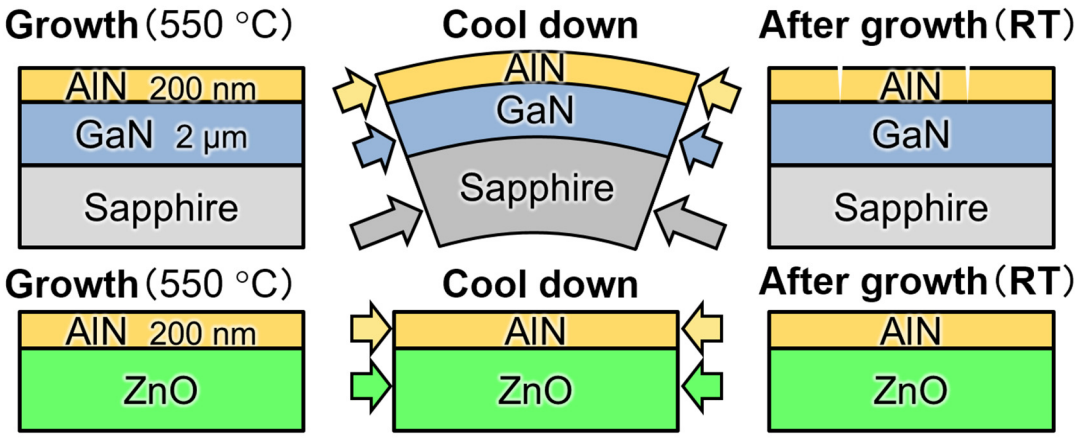

Figure 3.6. Cracking mechanism of AlN films.

shrunk during the cooling process. It leads the tensile stress in the GaN and AlN films at RT because sapphire has a large TEC than GaN and AlN as shown in Table 3-1 [59, 60]. In the case of the ZnO substrate, the TEC of ZnO is close to that of AlN. Therefore, it is expected that the crack does not occur for the AlN/ZnO structure.

Table 3-1. Thermal expansion coefficient of each material.

Material	Thermal expansion coefficient ($\times 10^{-6}$/K)
AlN	4.40
GaN	3.56
Sapphire	7.22
ZnO	4.57

A schematic view of the RHEED is illustrated in Fig. 3.7. The incident electron beam strikes the sample surface at a grazing angle. The electrons are energetic with a typical energy of E (10 - 50 keV). The corresponding amplitude of the wave vector k_0 for these high-energy electrons can be estimated using an equation (3.3):

$$E = \sqrt{\frac{\hbar^2 |k_0|^2}{m^*}}, \tag{3.3}$$

where m^* is the effective mass of the electron.

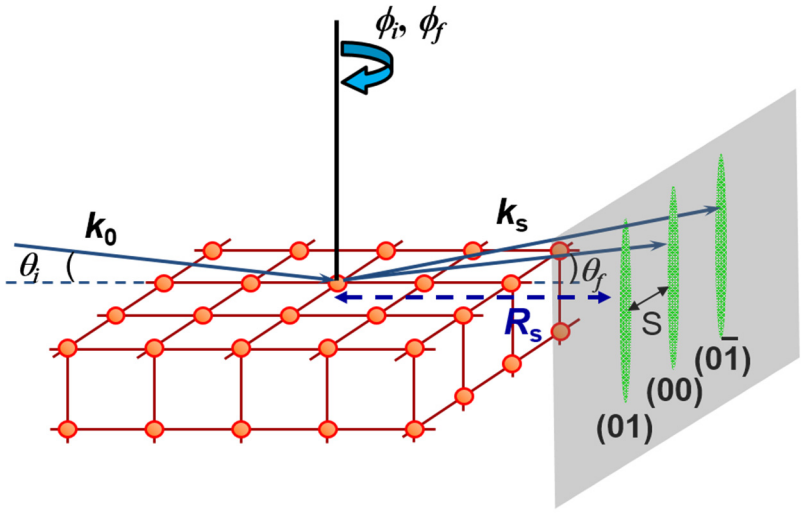

Figure 3.7. Schematic view of the RHEED. θ_i (θ_f) and ϕ_i (ϕ_f) are the incident and azimuthal angles of the incident (diffracted) beam. R_S is the distance between substrate and phosphor screen. S is the distance between the diffraction spots or streaks.

Without relativistic correction (which should be only a few percent for the energies of interest), the electron wavelength λ can be estimated by an equation (3.4):

$$\lambda(\text{Å}) = \sqrt{\frac{150}{E}}, \tag{3.4}$$

with E given in electron volts.

At the typical energies used in RHEED, the electron wavelength λ is approximately 0.05 - 0.1 Å, which is an order of magnitude smaller than the thickness of an atomic layer. The angle of incidence is typically set to a few degrees (~2°). At these grazing angles, the penetration depth is as small as a few atomic layers, which makes RHEED an extremely surface sensitive diffraction technique so the electrons are easily scattered by surface steps and terraces. The coherence length, which is the maximum distance between reflected electrons that are able to interfere, is determined by the beam convergence and the energy spread of the electrons, and is typically of the order of several hundred nanometers.

The electron gun and phosphor screen are located far from the sample to avoid any interference with the deposition process. In this geometry, electrons are scattered from

the crystal surface, resulting in a characteristic diffraction pattern on the phosphor screen. This pattern is simultaneously displayed and can be used to define the crystallographic surface structure of a growing thin film. RHEED spots are produced when the momentum of the incident beam and that of the diffracted beam differ by a reciprocal lattice vector G,

$$k_s - k_0 = \mathrm{G}, \tag{3.5}$$

where k_s and k_0 are the wave vectors of the diffracted and incident beams.

A useful geometrical representation of the conditions for diffraction in elastic scattering $|k_s| = |k_0|$, is provided by the Ewald sphere construction. Here, the reciprocal lattice of a 2D surface is a lattice of infinitely thin rods, perpendicular to the surface. The tip of the incident wave vector is attached to a reciprocal lattice rod. The Ewald sphere is defined by the sphere around the origin of k_0 with radius $|k_0|$ (equals $2\pi/\lambda$ for elastic scattering). The condition for diffraction is satisfied for all k_S connecting the origin of k_0 and a reciprocal lattice rod. For perfect surfaces, this result in diffraction spots lying on concentric circles, called Laue circles.

From the spot positions in a RHEED pattern of a perfect low index plane, one can determine the in-plane lattice constants. Using polar coordinates, the rectilinear projections of the scattering wave vector k_S can be written as follows.

$$k_{sx} = |k_0|\left(\cos\theta_f \cos\phi_f - \cos\theta_i \cos\phi_i\right), \tag{3.6}$$

$$k_{sy} = |k_0|\left(\cos\theta_f \sin\phi_f - \cos\theta_i \sin\phi_i\right), \tag{3.7}$$

and

$$k_{sz} = |k_0|\left(\sin\theta_f + \sin\theta_i\right) \approx |k_0|\left(\theta_f - \theta_i\right) \text{ (for small angles).} \tag{3.8}$$

k_{sx} and k_{sy} in the low index plane, k_{sz} perpendicular to the low index plane, θ_i and ϕ_i the incident and azimuthal angles of the incoming beam, and θ_f and ϕ_f the incident and azimuthal angles of the final (diffracted) beam as shown in Fig. 3.7. For the incident beam directed along a low index direction ($\phi_i = 0$), the lattice parameters d_x (parallel to the incident beam) and d_y (perpendicular to the incident beam) can be derived from the angles

of Bragg reflections using Eq. (3.6) by

$$\frac{n}{d_x} = \frac{1}{\lambda}\left(\cos\theta_f - \cos\theta_i\right), \tag{3.9}$$

where $\phi_f = 0$, that is, for intersections of the Ewald sphere with (h0) rods, and

$$\frac{n}{d_y} = \frac{1}{\lambda}\left(\cos\theta_f \sin\phi_f\right), \tag{3.10}$$

where n is the order of the reflection. The angles can be determined directly by dividing the relative on screen distances by the sample-to-screen distance R_S, assuming only small angles.

Figures 3.8(a) and 3.8(b) show the GaN[$1\bar{1}00$]//Al_2O_3[$11\bar{2}0$] azimuth RHEED patterns of as-grown AlN films grown at 3 Pa and the temperatures of 200 °C and 350 °C, respectively. The observed vertically elongated spot patterns of both samples are consistent with the wurtzite AlN structure at [$1\bar{1}00$] azimuth, where horizontal and vertical spot spaces correspond to 2/a and 2/c, respectively, and the ratio of wurtzite AlN lattice constants c/a is 1.6. The horizontal width of the spots indicates that the in-plane coherent domain size of PLD-grown AlN surface is less than 10 nm, which is probably caused by the lattice mismatch with the GaN template and low temperature growth. In such case, if the surface is flat, a streak pattern is observed owing to the shallow penetration depth (close to lattice constant c) of glazing-incidence electrons. The elongated-spot indicates that the surface is not so flat. The spotty pattern as the AlN films grown at 200 °C means a few surface-normal lattices contribute to the pattern as shown in Fig. 3.8(a). On the other hand, much longer length of the pattern was presented at the higher temperature of 350 °C as shown in Fig. 3.8(b).

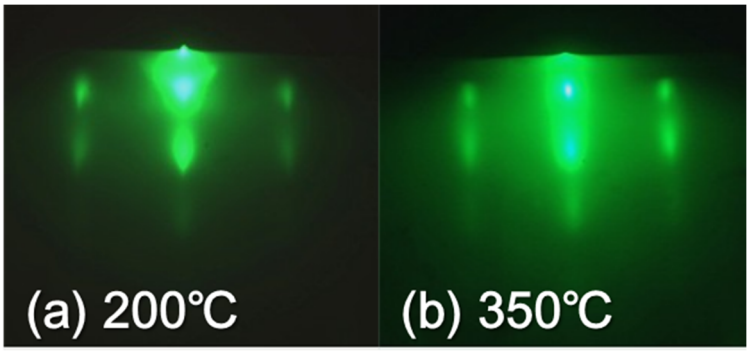

Figure 3.8. RHEED patterns at [1$\bar{1}$00] incident azimuth of AlN films on Ga-polar GaN templates grown by PLD at 3.0 Pa and (a) 200 °C and (b) 350 °C.

3.3.2 Single crystal AlN growth on ZnO substrate

The growth conditions of AlN films on Ga-polar GaN templates were optimized as the pressure of 3 Pa and 350 °C. Thus, at first the AlN growth on the ZnO substrate was also performed at 3 Pa and 350 °C. However, the AlN 0002 diffraction peak was not observed as shown in Fig. 3.9. To obtain a single crystalline AlN film on the ZnO substrate, the pressure conditions had to be arranged. The pressure was fixed at 4 Pa because the pressure was optimized at the AlN growth on the GaN template. The temperature was varied at 350 °C, 450 °C and 550 °C. For the temperature of 350 °C and 450 °C, there was no AlN related diffraction peak. For the AlN film grown at 550 ºC, The AlN 0002 peak appeared at the position corresponding to the lattice spacing 0.40% larger than the *c*/2 of bulk AlN as shown in Fig. 3.9. The surface of the PLD-grown AlN film grown at 550 °C exhibits the step-terrace structure without crack in the AFM image shown in Fig. 3.10(a).

In order to confirm the crystal structure of AlN, EBSD was measured. In the phase image, the wurtzite structure, corresponding to the red color, was confirmed as shown in Fig. 3.10(b). The Kikuchi pattern of AlN films, which has sixfold rotational symmetry around the surface-normal zone axis, coincided with that of the hexagonal AlN structure as shown in Fig. 3.10(c).

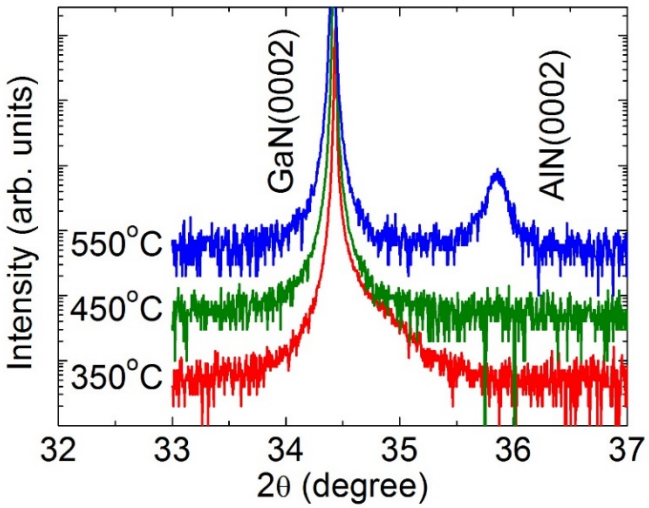

Figure 3.9. XRD 2θ-ω scan results of AlN films on ZnO substrates grown at 4 Pa and temperatures at 350 °C, 450 °C and 550 °C.

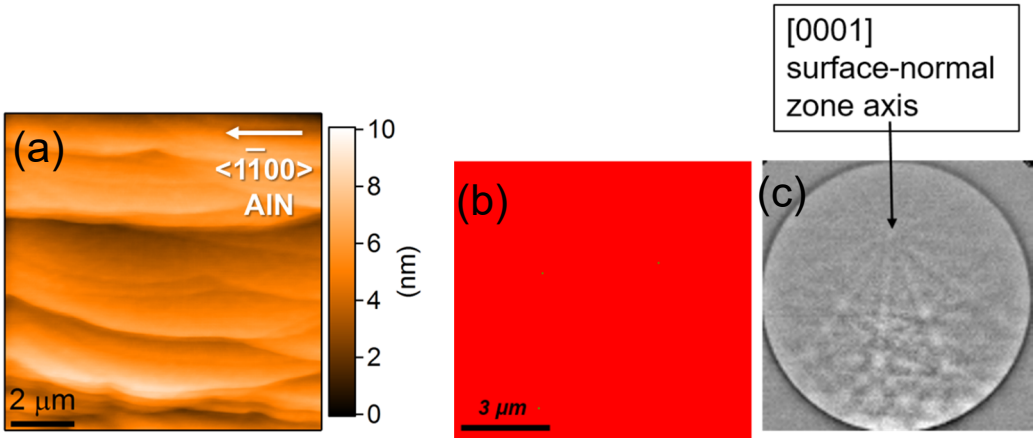

Figure 3.10. (a) AFM image, (b) EBSD phase image (red: wurtzite, green: zincblende), and (c) Kikuchi pattern of PLD-grown AlN film grown on ZnO substrate at 4 Pa and 550 °C.

3.3.3 Investigation of strain in AlN films

To investigate the strain in the AlN films, reciprocal space mapping (RSM) was measured. XRD 2θ-ω scan has a limitation which can only evaluate the out-of-plane lattice constants. This measurement is performed by 2θ-ω scan in concert with ω scan. The abscissa and ordinate of the resultant image, Qx and Qy, correspond to in-plane and out-of-plane, respectively. An illustration of the RSM for the AlN/ZnO film is shown in

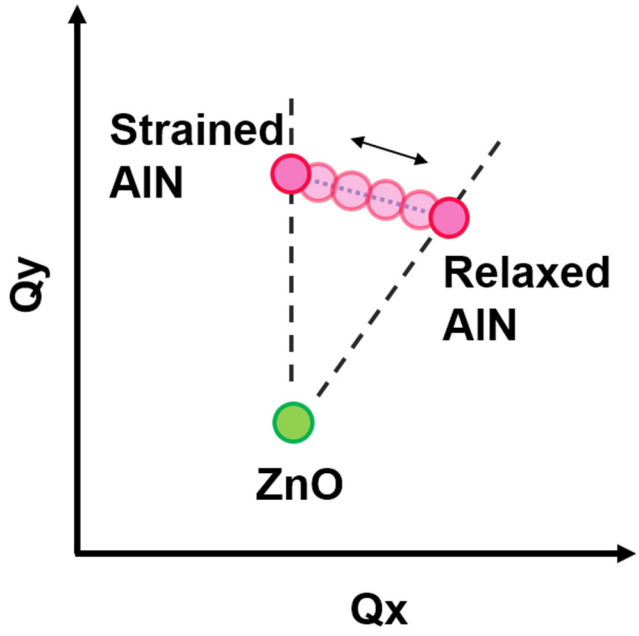

Figure 3.11. Schematic diagram of asymmetric RSM of AlN/ZnO.

Fig. 3.11. The AlN diffraction is normally located upper than the ZnO diffraction because the lattice constants of AlN is smaller than those of ZnO. If the AlN film is coherently grown on a ZnO substrate, the AlN diffraction is observed along the vertical line because of the consistent of the in-plane lattice constant. On the other hand, the AlN diffraction is observed along an inclined line toward the right-hand side from the ZnO diffraction owing to the smaller AlN lattice. RSM method is also utilized to investigate the alloy composition of the InGaN film. It will be explained in Chapter 4 for the subsequent InGaN growth.

RSM was used to investigate the strain of the AlN films. RSM around the GaN $10\bar{1}4$ and AlN $10\bar{1}4$ diffractions are shown in Fig. 3.12. For the AlN film grown at 350 °C and 3 Pa, two peaks were observed. The lower left peak with high intensity (blue to red cross lines) is corresponding to the GaN template. The upper right peak with low intensity (blue in white dashed-circle) is corresponding to the AlN films. The AlN diffraction peak position shifted close to that from the GaN template as the growth pressure is increased.

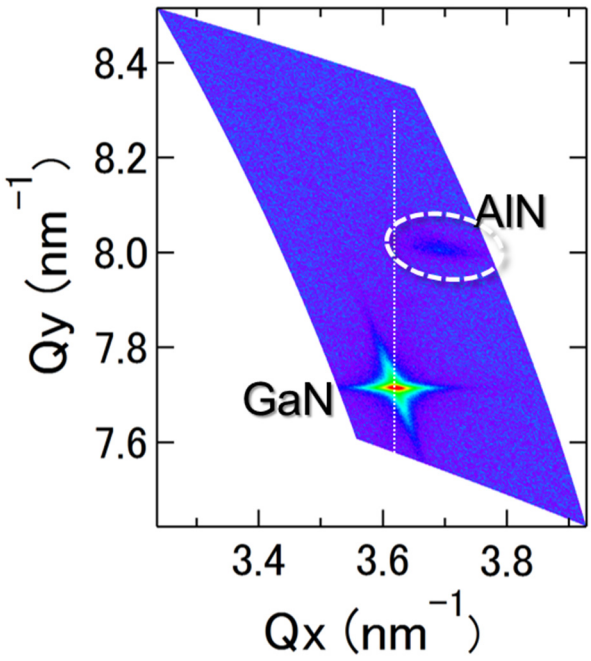

Figure 3.12. RSM around GaN $10\bar{1}4$ diffraction for PLD-grown AlN film on GaN template at 350 °C and 3 Pa.

Figure 3.13 shows the experimentally-obtained *a*- and *c*-axis lattice constants of PLD-grown AlN films. The growth conditions are also indicated in Fig. 3.13. The lattice constants *c* of the grown AlN films on the GaN templates were entirely larger than those of strained AlN to GaN. And the lattice constants *a* of the AlN films were partly relaxed from that of the GaN template. All the samples have larger volume than bulk AlN as shown in Fig. 3.13. These results appear when the films include an impurity [61-64]. The host atoms were relaxed by the adjacent impurities. Then the lattice parameter is changed. From Fig. 3.13, the diffraction peak position from the AlN film grown at 3 Pa and 350 °C is nearest to that of the bulk AlN except for the cracked AlN films grown at 550 °C. It is concerned that the optimized conditions for the AlN film growth on the GaN template.

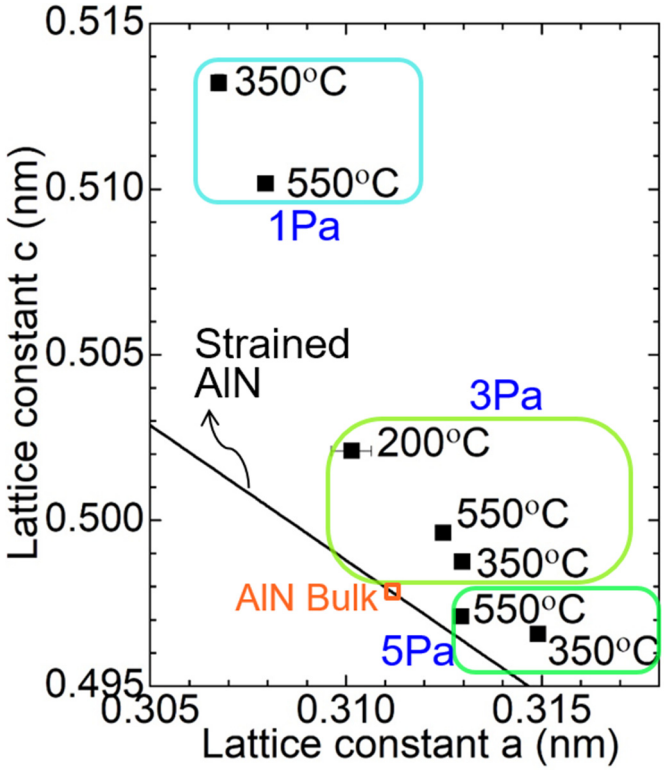

Figure 3.13. Lattice constants *a* and *c* for PLD-grown AlN films on GaN templates. Solid line shows calculated lattice constants of AlN with in-plane strain.

An X-ray photoelectron spectroscopy (XPS, Kratos AXIS-ULTRA) analysis on the AlN films was carried out to obtain the information about impurity and bonding of AlN. The X -ray source of Al Kα (E_{photon} = 1486.7 eV) was operated at 15 kV and 10 mA. A spot size of 110 μm diameter was adopted to analyze the photoelectrons. The background pressure of the chamber was 2×10^{-10} Torr. An Ar ion beam bombardment was performed to remove the surface contaminations of the samples at the pressure 5×10^{-8} Torr.

Table 3-2. PLD growth conditions of the AlN films.

Growth pressure (Pa)	Growth temperature (°C)
1	550
3	350
3	550
5	550

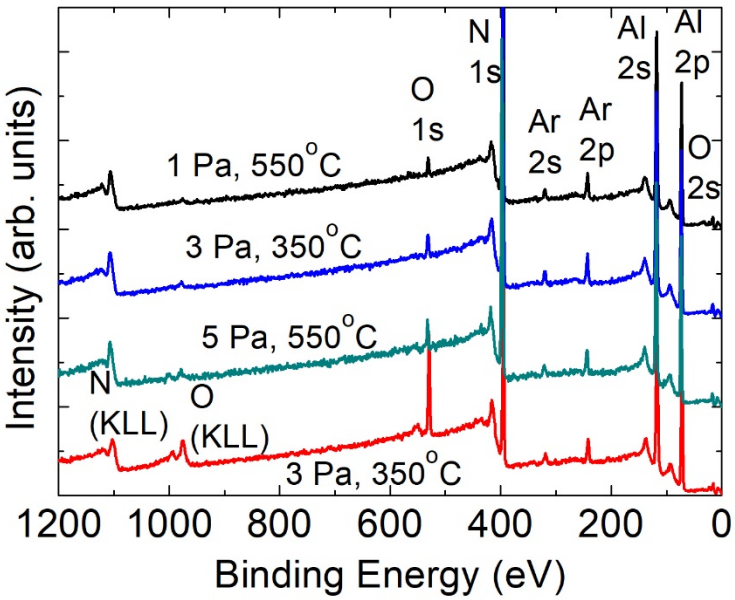

Figure 3.14. Survey mode scan of AlN films after etching for 30 seconds.

Hence, we suspected the existence of impurity in the AlN films from the RSM measurements and tried to measure X-ray photoelectron spectroscopy (XPS) to clarify the composition of the material. Figure 3.14 shows the survey mode scan of the AlN films grown at the indicated conditions. The narrow scan was performed for more details as shown in Fig. 3.15. The graph shows binding energy of (a) Al 2p and (b) N 1s, respectively. In the Al 2p peak, an asymmetric single curve was separated into the two symmetric peaks by fitting a curve. AlN grown at 3 Pa 350 °C shows the relatively higher intensity of Al-O (red line, 74.2 eV) bonding and lower intensity of Al-N (blue line, 73.4 eV) bonding as shown in Fig. 3.15(a). The grown AlN films at 3 Pa and 350 °C, the Al-O bonding peak has more than twice intensity compared with the samples grown at other conditions. In contrast, the intensity of the Al-N bonding was relatively decreased at 350 °C as shown in Fig. 3.15(a). It is indicating that the vigorous oxidization was occurred at the lower temperature. The spectra of the N 1s peaks are shown in Fig. 3.15(b). In this case, observed peaks were separated into 3 peaks by fitting a curve. Among them, the Al-N (red line, 396.5 eV) bonding was dominant. The sub peak of N 1s has a binding energy of 395.1 eV (pink line) while other sub peak of N 1s appeared at 398.1 eV (blue line). The Al-N bonding maintained a similar intensity when the temperature or pressure is

changed. It is postulated that the origin of the sub peak of 398.1 eV probably comes from a formation of three component system such as Al-O-N. The nitrogen sources arrive at the surface of the substrate with ions (N^+ or N_2^+) by the plume in PLD. These ions incorporated in the growing film and increase their coordination to Al-species until a stable single bonded N-Al structure is established in wurtzite phase of AlN. At that time the binding energy range of 397.6 eV to 398.6 eV is observed. Constales *et al*. concluded about this that N-N bounded defect structures are to be expected in thin film deposition methods that proceed layer by layer [65].

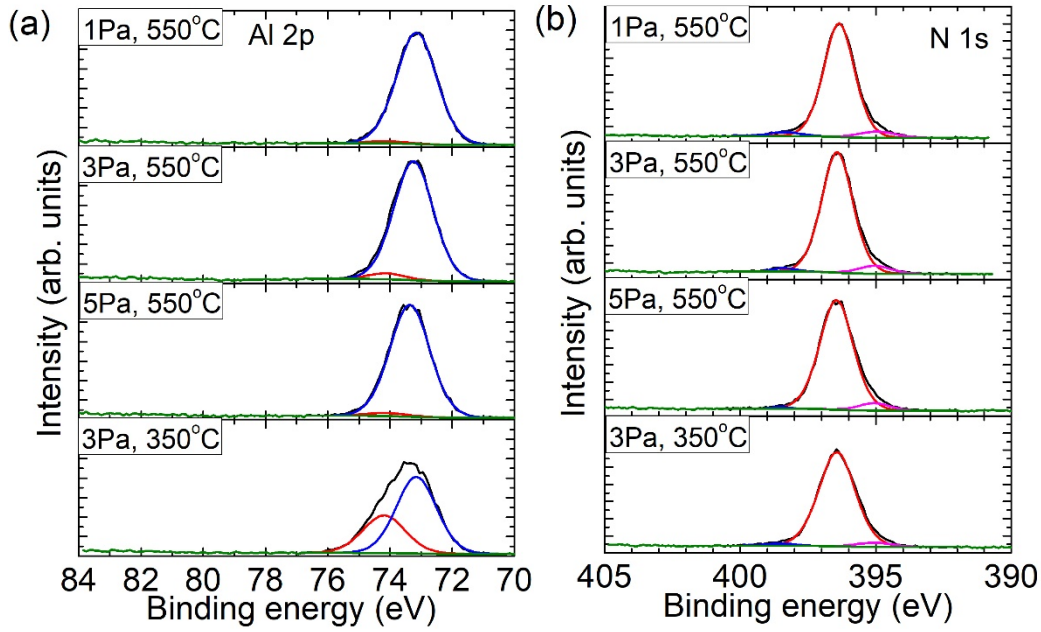

Figure 3.15. Narrow XPS scan of AlN films with respect to (a) Al 2p and (b) N 1s.

Whether the existence of the oxygen is in entire AlN layer or just near a surface must be confirmed. Therefore, the XPS depth profile of the AlN film grown at 1 Pa and 550˚C as a representative was measured and its result is shown in Fig. 3.16. Carbon was detected on the surface but it disappeared from the 2 nm etched surface. However, O is detected in the entire AlN layer with 1.97% of O at. %. Then, O is disappeared in GaN layer. It means there is no reaction in the interlayer between AlN and GaN when we transfer the reactor.

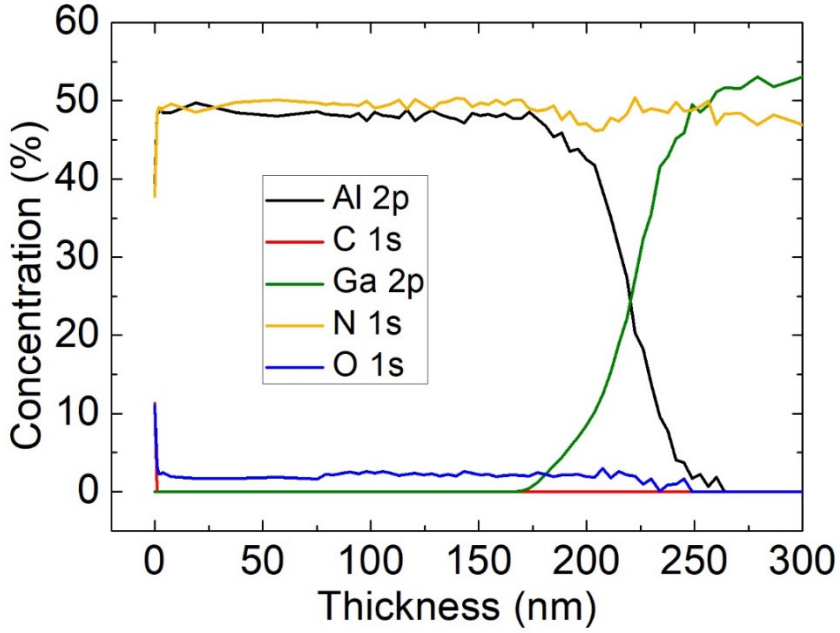

Figure 3.16. XPS depth profile of AlN grown at 550 °C and 1 Pa.

RSM of the grown AlN films on the ZnO substrates were also measured. RSMs around the ZnO $10\bar{1}4$ and AlN $10\bar{1}4$ diffractions are shown in Fig. 3.17. For the AlN film grown at 550 °C and 4 Pa, two peaks were observed. The blue spot of the top AlN films are not in vertical alignment with the spot of the ZnO substrate, indicating the relaxed AlN growth on the ZnO substrate. Figure 3.18 shows the lattice constants *a* and *c* for PLD-grown AlN films on the ZnO substrate and the GaN template. The lattice constants of the bulk AlN crystal is also plotted. The AlN film grown on the ZnO substrate has the lattice constants *a* and *c* of 0.3109 nm and 0.50165 nm, respectively. The AlN film grown

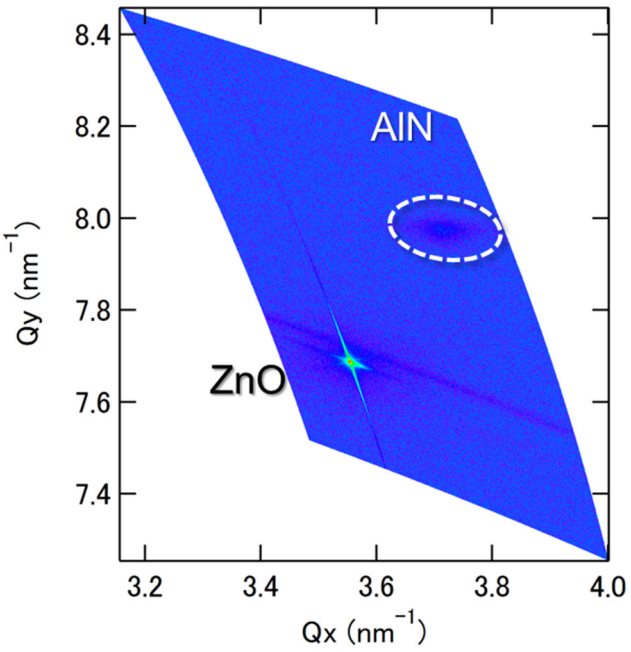

Figure 3.17. RSM of GaN $10\bar{1}4$ diffraction for AlN film on ZnO substrate grown at 350 °C and 4 Pa.

on the GaN template has the lattice constants *a* and *c* of 0.31308 nm and 0.49822 nm, respectively. Those values are larger than those of the bulk AlN crystal. It is expected that the both of the AlN films grown on the GaN template and the ZnO substrate have large amount of unintentional impurities such as oxygen. High density impurities change the lattice constants.

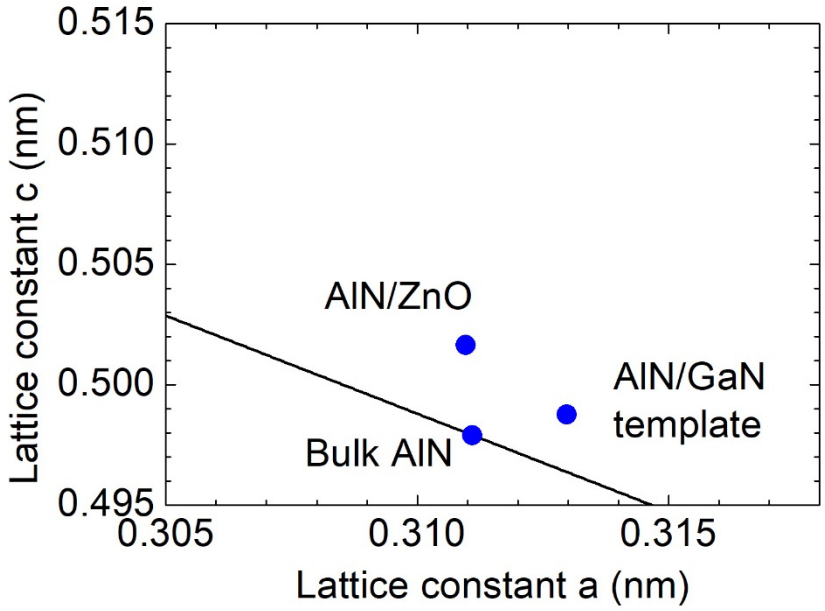

Figure 3.18. Lattice constant *c* as a function of the lattice constant *a* for bulk AlN, PLD-grown AlN film on GaN template and PLD-grown AlN film on ZnO substrate.

3.4 Summary

In this chapter, the AlN films were introduced to suppress the decomposition of the ZnO substrate during MOVPE growth.

- Single crystalline AlN films were grown on an MOVPE-grown GaN template and a ZnO substrate by PLD.
- For the AlN film grown on a GaN template, the atomically flat surface without any cracks was obtained when the growth temperature was between 200 °C and 550 °C.
- For the AlN film grown on a ZnO substrate, the optimized conditions were 4.0 Pa and 550 °C. Low temperature growth deteriorated the surface morphology. No cracks were observed.
- The AlN film is applicable as an epitaxial protection layer for the epitaxial growth of InGaN films by MOVPE.

Chapter 4. Back-coating of ZnO substrate

4.1 Introduction

This chapter describes the study on the protection of the side and the bottom of a ZnO substrate. The protection layers such as the low-temperature GaN buffer layer and the Al_2O_3 one have been already reported for the MOVPE growth of InGaN films on ZnO substrates [66-68]. Since the impurity comes from the bottom of the ZnO substrate during the growth with MOVPE, bottom of the ZnO substrate was coated by the sputtering system. In this study, AlN and SiO_2 films were utilized to protect a ZnO substrate. The AlN and SiO_2 films were sputtered in various thicknesses.

4.2 Necessity of back-coating

During the InGaN growth by MOVPE, ZnO substrates were decomposed in the atmosphere of MOVPE. Figures 4.1(a) and 4.1(b) show optical microscope (OM) images of the ZnO substrate and the InGaN film on the ZnO substrate grown by MOVPE, respectively. ZnO strongly reacts with H_2, which is used as a carrier gas or decomposed from NH_3 source gas. In order to suppress the decomposition of the ZnO substrates, back-coating of the ZnO substrates is necessary.

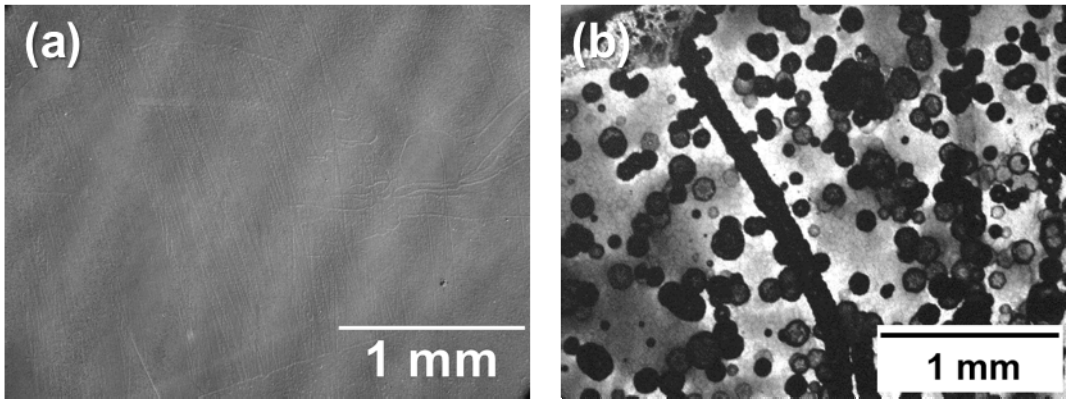

Figure 4.1. OM images of surfaces (a) before and (b) after InGaN growth on a bare ZnO substrate by MOVPE.

4.3 Experiments

Both of the AlN and SiO_2 films of thickness 800 nm were formed on a back side of the ZnO substrate by radio-frequency (RF) sputtering system at room temperature. The

sputtering system (Anelva SPF-210A) is shown in Fig. 4.2.

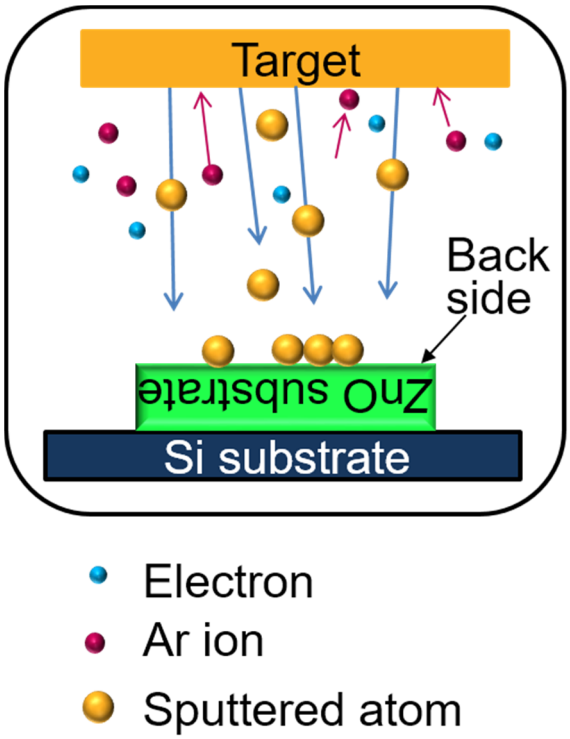

Figure 4.2. Schematic of sputtering in a reactor for the back-coating.

The background pressure was reduced around 3×10^{-4} Pa. Ar gas was supplied to ignite the plasma in the chamber. Al (99.99%), SiN (99.99%), and SiO_2 (99.99%) were used as the targets of AlN, SiN and SiO_2, respectively. The AlN films were sputtered in an ambient of Ar 3 sccm and N_2 5 sccm at 2.0 Pa with a RF power of 150 W. The SiO_2 films were sputtered in an ambient of Ar 10 sccm at 5.0 Pa with a RF power of 100 W. The sputtering rate of AlN and SiO_2 was 10 nm/min and 15 nm/min, respectively. All the deposition conditions of the materials are shown in Table 4-1. The protection layers, SiN, AlN, SiO_2 and AlN/SiO_2, were deposited on the backside of the ZnO substrates by sputtering in order to protect the backside of the ZnO substrates. Subsequently, the

Table 4-1. Sputtering conditions for each material.

Protection layer		SiO_2	SiN	AlN
Target		SiO_2	Si_3N_4	Al
Gas (sccm)	Ar	10	10	3
	N_2	–	4	5
Pressure (Pa)		5	5	2
RF power (W)		100	100	150
Thickness (nm)		800	800	800

deposited films were annealed in the air atmosphere at 800 °C for 60 minutes. The surface morphology was observed with an optical microscope.

4.4 Effect of protection layer

Except the SiN, temperature resistant of the protection layers were confirmed by annealing in the air atmosphere at 800 °C, which is consistent with the InGaN growth temperature. Figure 4.3 shows an optical microscope (OM) image of the SiN surface. In the case of the SiN films, high-density pits were already distributed on a surface even though annealing was not carried out. Therefore the SiN film was excluded for a back coating material.

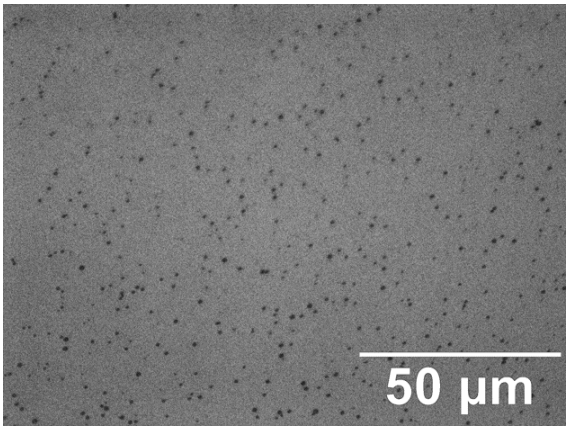

Figure 4.3. OM image of sputtered SiN films before annealing.

For the SiO_2 films, the pits were observed after the annealing as shown in Fig. 4.4(b). For the AlN films, the surface morphology showed hexagonal feature as shown in Fig. 4.5(a). This phenomenon appears when the grown films have the wurtzite phase [69-71]. It implies that the partial hexagonal features exist in the sputtered AlN films; the exfoliation occurs from those boundary as shown in Fig. 4.5(b).

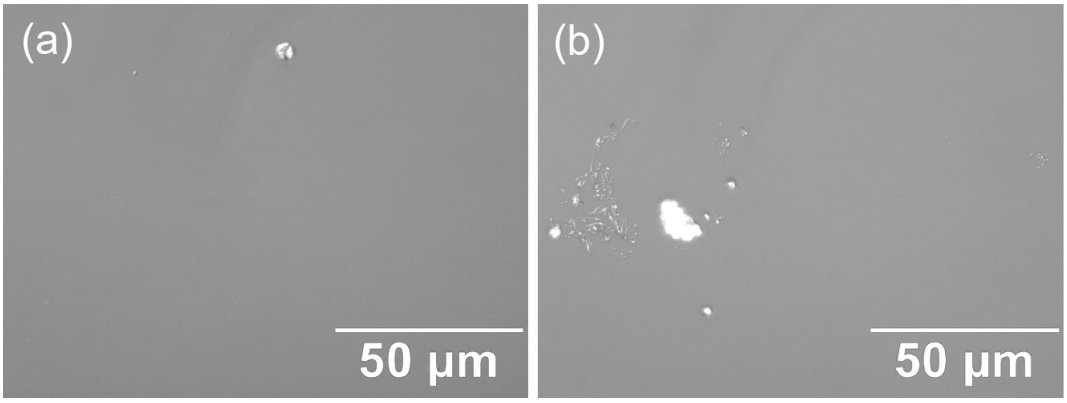

Figure 4.4. OM images of sputtered SiO_2 films (a) before and (b) after annealing.

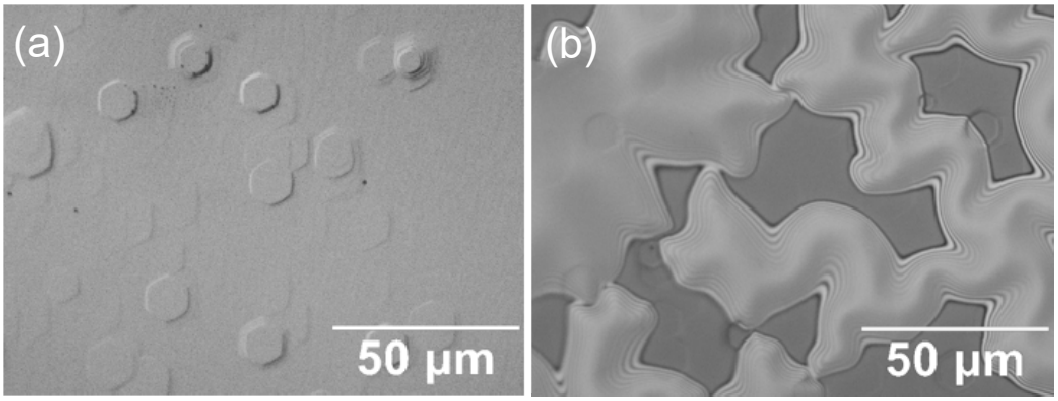

Figure 4.5. OM images of sputtered AlN films (a) before and (b) after annealing.

To confirm the initial reaction of the sputtered film, a 200-nm-thick AlN film was prepared and its stability in the NH_3 atmosphere of the MOVPE reactor was investigated. The sample temperature and the reactor pressure were maintained at 800 °C and 650 Torr for 60 minutes, respectively. NH_3 was also supplied with 15 slm. Figure 4.6 shows an OM image of the sample after annealing in the NH_3 atmosphere of the MOVPE reactor. It is distinctly revealed that the AlN film starts to exfoliate from the hexagonal structures. As mentioned before, the hexagonal features appear when the film is a wurtzite phase. It is

necessary to remove the hexagonal features to overcome an exfoliation of the film, since the exfoliation occurs from the hexagonal features. Therefore amorphous SiO_2 films were preferentially sputtered and then AlN sputtering was followed to avoid the formation of the hexagons.

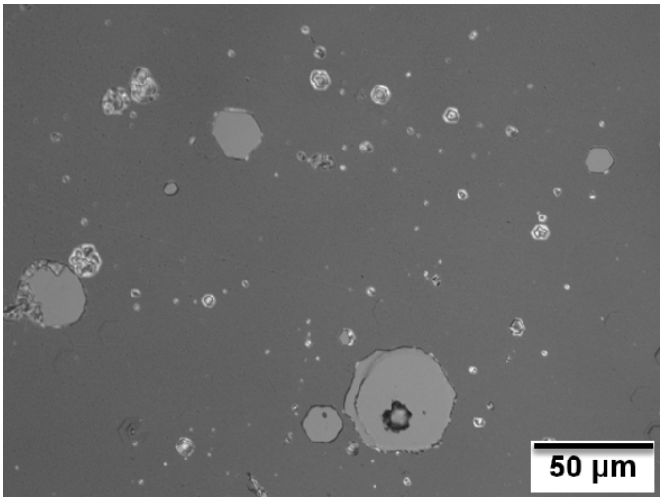

Figure 4.6. OM image of AlN film after test in NH_3 atmosphere of the MOVPE reactor.

In order to confirm the role of a protection, the thicknesses of the AlN films were varied as 200 nm, 400 nm, 600 nm, and the thickness of the SiO_2 films was fixed to 800 nm. Table 4-2 summarizes the stability of the samples after annealing. After annealing, the pits were distributed on the annealed surface when the thickness of the AlN film was less than 800 nm as shown in Fig. 4.7.

Table 4-2. Relationship between thickness of AlN/SiO_2 and protection of the back side.

SiO_2 Thickness (nm)	AlN Thickness (nm)	Protection
800	200	X
	400	X
	600	X
	800	O

The pits and hexagonal features disappeared at the surface when the thicknesses of the both films were 800 nm. The surface images of the AlN films before and after annealing are shown in Figs. 4.7(a) and 4.7(b), respectively. This result shows that the

amorphous SiO_2 film makes the AlN film without hexagonal features. Furthermore, an amorphous AlN film makes to avoid the decomposition of the ZnO substrate by the annihilation of the hexagonal boundary as shown in Fig. 4.8.

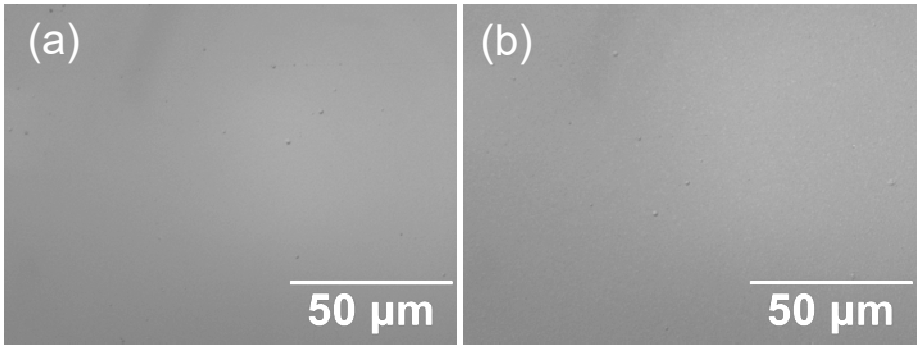

Figure 4.7. OM images of sputtered AlN/SiO_2 films
(a) before and (b) after annealing.

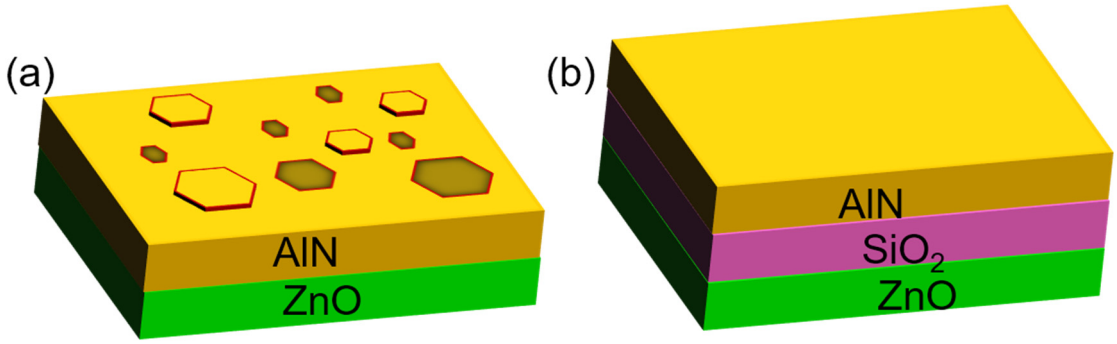

Figure 4.8. Schematics of sputtered surface morphology
for (a) single crystal and (b) amorphous films.

4.5 Summary

In this chapter, a protection layer for the back side of the ZnO substrate was introduced.

- Each single layer is not resistant at the growth temperature.
- The AlN layer includes hexagons on a surface and the exfoliation occurred at the boundary of the hexagonal features.
- The protection layer for the back side of the ZnO substrate without any exfoliation was achieved by inserting a SiO_2 amorphous layer, between the ZnO substrate and the AlN layer.

Chapter 5. Optimization of MOVPE InGaN growth and improvement of InGaN crystal quality

5.1 Introduction

The MOVPE growth of InGaN on a ZnO substrate has been already reported [72]. Since ZnO is not resistant to the reducing MOVPE-ambient of hydrogen (H_2) and ammonia (NH_3) at high temperature [73-75], the growth temperature has to be lowered by 200 °C in comparison with the usual growth temperature of InGaN on a sapphire substrate [76]. The surface morphology of an InGaN layer epitaxially grown at such low temperature becomes rough and its crystalline quality has to be still improved [77]. In this study, by introducing the protection layer, a high quality InGaN epitaxial layer on a ZnO substrate was demonstrated. In addition, an InGaN epitaxial film lattice-matching to ZnO is grown on a ZnO substrate and its epitaxial film is characterized.

5.2 InGaN growth by MOVPE

InGaN layers have been simultaneously grown on ZnO substrates and c-plane sapphire with 0.2° off-cut around *a*-axis by MOVPE. The MOVPE system is composed of a gas supply system, a quartz reactor, a RHEED chamber, a load-lock chamber, and an exhaust system. A susceptor coated with SiC is used to mount a substrate and it is heated by a RF coil. Metalorganic (MO) sources are supplied for the group-III precursors. As group-III precursors, Triethylgallium (TEGa) and Trimethylindium (TMIn) are used for Ga and In precursors, respectively. NH_3 is used for a N source. N_2 is used for a carrier gas. The simplified illustration of the MOVPE reactor is shown in Fig. 5.1.

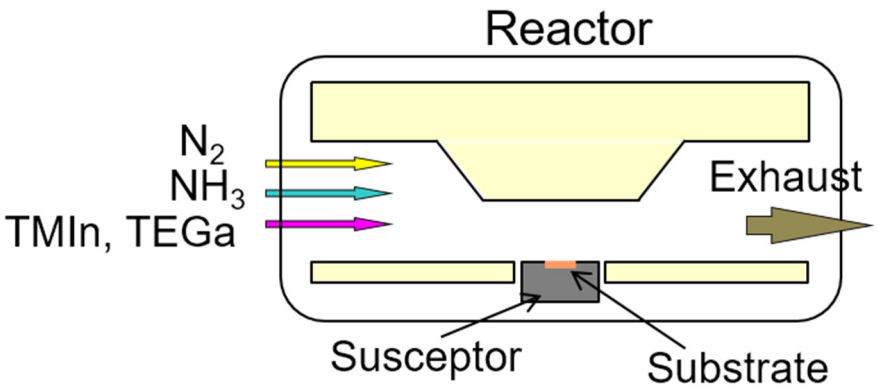

Figure 5.1. Reactor of MOVPE system.

MO sources are bubbled and transported to the reactor with N_2 carrier gas. The amount of the MO sources supplied has to be accurately and precisely controlled because the amount of an MO source transportation depends on the flow rate of a carrier gas, and the temperature and the pressure of a bubbler. For this purpose, a mass-flow controller (MFC), a pressure regulator, and a thermostatic bath for group-III sources are equipped. Besides, Tomas Swan Epison system (Epison II) was introduced in order to accurately control to the molar amounts of TMIn and TEGa. This reason is that the TMI is a solid source and its flow rate strongly depends on its surface area. For TEG, its flow rate is small. Epison II can measure the velocity of ultrasonic wave in the vapor amount of TMI. This velocity is proportional to the concentration of TMI in the carrier gas. The MFC controls the total flow of MO source and carrier gas molecules per unit of time. Epison II keeps the flow of MO source molecules, and constant even the temperature and the pressure of the change. Therefore Epison II makes it possible to the reproduces by the accurate source supply.

In the InGaN growth process shown in Fig. 5.2, the growth conditions of InGaN grown on a ZnO substrate and a sapphire substrates are shown in Table 5.1 and Table 5.2, respectively. The gas flow sequence consists of 6 steps. The first step, “gas- regulation flow 1”, is that each flow rate of NH_3 and N_2 is increased from 0 to 15.0 slm and 1.5 to 11.0 slm, respectively. The second step, “temperature up”, is the duration to raise up the surface temperature. The third process, “wait”, is the duration for which all the gas flows and the surface temperature become stable. An MO source is bubbled during this moment. In the fourth step, InGaN is grown with a high V/III ratio of 19,490 in a N_2 flow at 800

°C. The fifth step, “gas-regulation flow 2”, is the duration to reduce each flow rate of NH_3 and N_2 from 15.0 to 0 and 11.0 to 1.5 slm, respectively. The final step, “cooling down”, is waiting for cooling down. During the growth, the reactor pressure is fixed at 650 Torr. The 500-nm-thick *c*-plane InGaN films were grown on ZnO substrates. H_2 carrier gas is completely prevent a ZnO substrate from being gas-etched. The high V/III ratio of about 15000 is maintained to avoid the generation of the indium droplet. Those growth conditions are shown in Table 5-1. In the case of the InGaN growth on a sapphire substrate, the indium composition is controlled by changing the surface temperature. The conditions of the InGaN growth on a sapphire substrate are shown in Table 5-2. The other growth conditions such as the V/III ratio, TMIn/(TMIn + TEGa), NH_3, are the same as ones for a ZnO substrate.

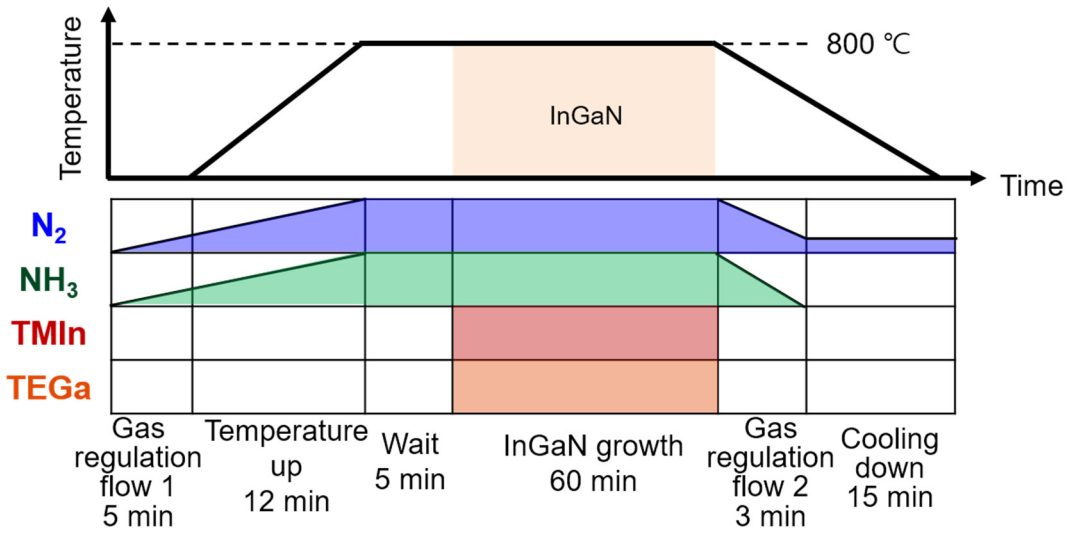

Figure 5.2. InGaN growth procedure with MOVPE.

Table 5-1. Growth conditions of InGaN on ZnO substrate.

Growth parameter	value
Growth temperature (°C)	750 - 800
Growth time (min)	60
TEGa (µmol/min)	15.5 – 25.5
TMIn (µmol/min)	19.2 – 29.2
NH_3 (slm)	15
TMIn + TEGa (µmol/min)	44.82
TMIn / (TMIn + TEGa)	0.43 - 0.65
V/III ratio	14940
Reactor pressure	650

Table 5-2. Growth conditions of InGaN on sapphire substrate.

Growth parameter	value
Growth temperature (°C)	770 – 810
Growth time (min)	60
TEGa (µmol/min)	15.5
TMIn (µmol/min)	29.3
NH_3 (slm)	15
TMIn + TEGa (µmol/min)	44.82
TMIn / (TMIn + TEGa)	0.65
V/III ratio	14940
Reactor pressure	650

5.3 Investigation of InGaN films

In order to evaluate the role of PLD-AlN and AlN/SiO_2, the MOVPE growth temperature of InGaN was varied to 750 °C, 800 °C, and 850 °C. The surface morphologies of InGaN were observed by a differential interference optical microscope as shown in Fig. 5.3. The InGaN films grown at (a) 750 °C and (b) 800 °C were transparent and dark with the naked eye, respectively. A dark color originates from the high InN mole fraction of InGaN films because an InGaN film with the higher InN mole fraction has an optical absorption edge at the longer wavelength. In the case of the InGaN films grown at (c) 850 °C, the InGaN film was exfoliated from a substrate, and the ZnO substrate deteriorated whereas the amorphous AlN/SiO_2 films kept the backside of a ZnO substrate.

The surface of a 500-nm-thick InGaN film grown at 750 °C was rough. This means that the temperature is insufficient for the migration of adatoms on the top surface. Raising up the growth temperature to 800 °C, the step flow growth occurred and the surface of InGaN was improved to be smooth.

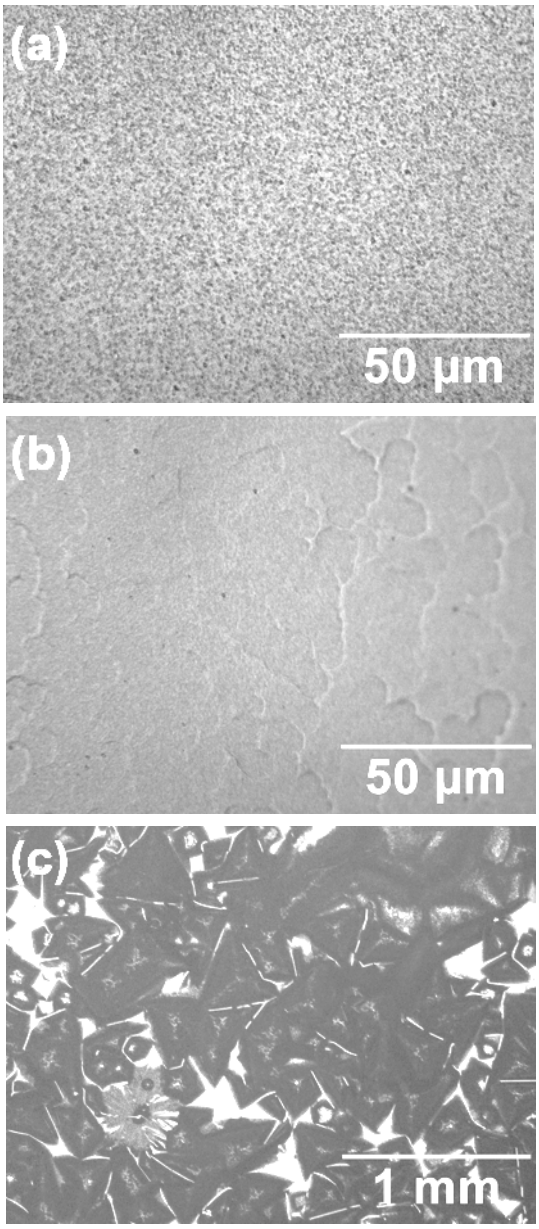

Figure 5.3. Surface morphologies of InGaN surface grown at (a) 750 °C, (b) 800 °C, and (c) 850 °C.

Figure 5.4 shows the XRD spectra of 2θ-ω and Φ for an InGaN film grown at 800 °C. From the 2θ-ω scan result, the InGaN films grown on AlN/ZnO oriented to the direction of <0001>. The InGaN film have the six-fold azimuthal symmetry consistent with the wurtzite crystal structure.

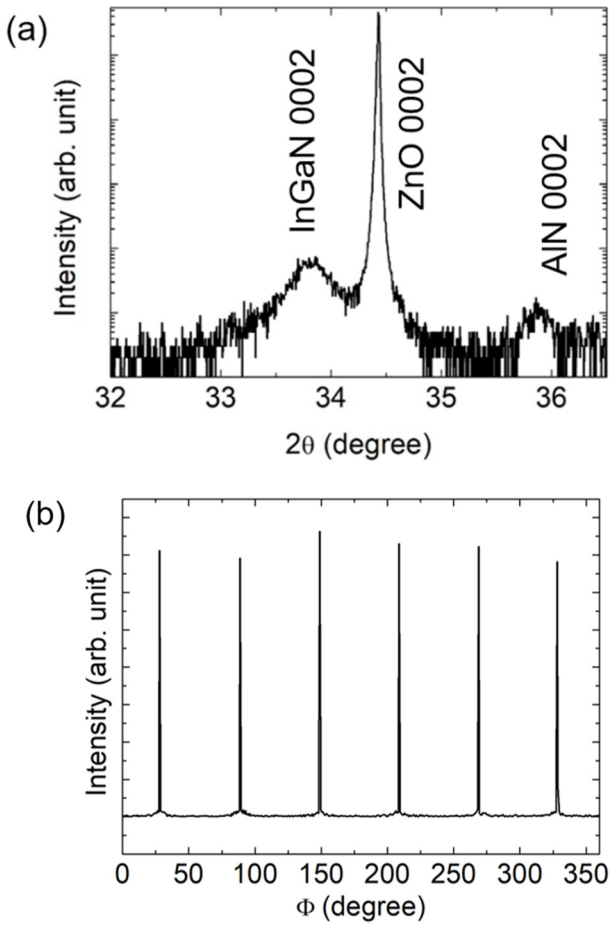

Figure 5.4. XRD spectra (a) 2θ-ω scan and (b) Φ scan of InGaN.

The asymmetric diffraction plane is used to estimate the InGaN composition and its strain. In the RSM, the strain of InGaN can be estimated by the location of the InGaN peak as explained in the following. If an InGaN film is coherently grown on a substrate, the InGaN diffraction peak is vertically aligned with the ZnO peak. In this case, the InGaN film is usually strained except for the lattice-matching InGaN with the InN mole fraction of 0.18 as shown by a red circle in Fig. 5.5. For this case, the in-plane lattice constant is identical with that of ZnO. On the contrary, for a fully relaxed InGaN film, the InGaN peak moves along the oblique line in Fig. 5.5 depending on the InN mole fraction. At the cross point of the two lines, *i.e.* red circle, InGaN fully relaxes and lattice matches to ZnO. In the RSM of InGaN for $10\bar{1}5$ diffraction, a strong ZnO diffraction was observed at the upper location as shown in Fig. 5.6. The diffraction below the ZnO one corresponds to the diffraction of InGaN. From the coordinate at the highest intensity of the InGaN

diffraction, its lattice constants are evaluated as a = 0.325 nm and c = 0.528 nm. These values correspond to the lattice constants of fully relaxed $In_{0.18}Ga_{0.82}N$. This shows that the InGaN film lattice-matched to ZnO is successfully grown on a ZnO substrate. It was demonstrated in this chapter that the lattice matched InGaN growth on a ZnO substrate by MOVPE.

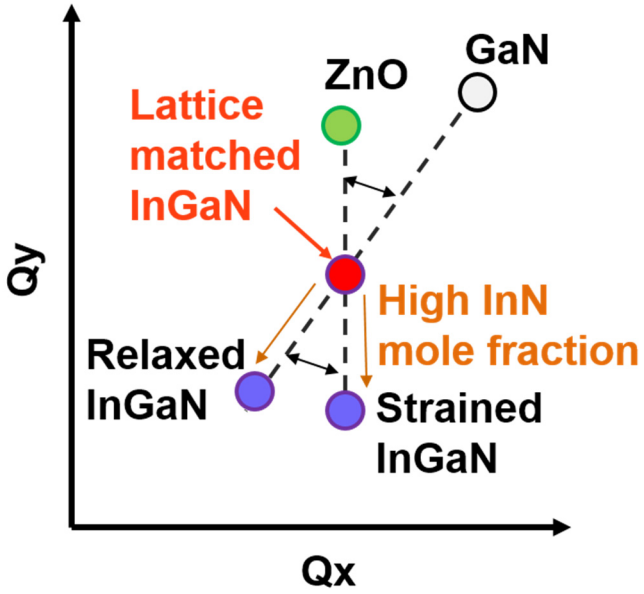

Figure 5.5. Schematic diagram of asymmetric diffractions of ZnO and InGaN in RSM.

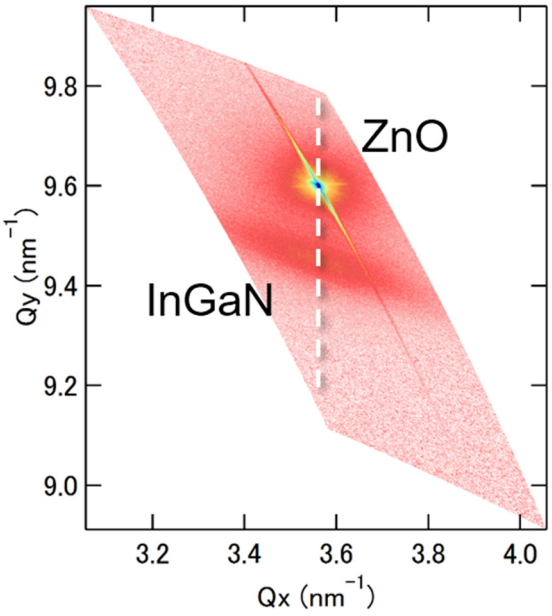

Figure 5.6. ZnO $10\bar{1}5$ diffraction RSM for InGaN film grown on ZnO substrate.

5.4 Summary

In this chapter, the InGaN film was grown on a ZnO substrate by MOVPE.

- By introducing the PLD-AlN films and back coating AlN/SiO_2 films, the decomposition of a ZnO substrate was suppressed.
- A single crystalline InGaN film was grown on the AlN/ZnO structure.
- The growth of the lattice matched InGaN film on the ZnO substrate by MOVPE was demonstrated.

Chapter 6. Conclusions

6.1 Summary

The thesis is summarized in order of process in this chapter.

Chapter 2: Fabrication of ZnO substrate by hydrothermal growth method

In order to obtain the ZnO substrates, ZnO crystals were grown by the hydrothermal method with a growth rate of 0.227 mm/day. Then 10 × 10 mm^2 *c*-plane ZnO substrates were fabricated by dicing, CMP, and annealing. The substrates had high transparency with a transmittance of 73 – 80% and rough surfaces with scratches caused during the CMP process. To improve the surface roughness, the ZnO substrates were annealed at 1150 °C for 4 hours in a box made of ZnO ceramics which could suppress the evaporation of Zn from ZnO. The step and terrace structures appeared at the surface after the annealing. In this chapter, ZnO substrates could be basically prepared for the epitaxial growth with the screw TDDs of 8×10^2 cm^{-2} and the edge TDDs of 4×10^3 cm^{-2}.

Chapter 3: Epitaxial growth of AlN protection layer by PLD

To suppress the decomposition of the ZnO surface during the MOVPE growth, a 200-nm-thick single-crystalline AlN film was epitaxially grown by PLD. An atomically flat surface was obtained at the growth temperature from 200 to 550 °C. Cracks appeared in the AlN film when the growth temperature was higher than 550 °C. From the XRD and EBSD measurements, the PLD-grown AlN film was *c*-plane-oriented single crystalline wurtzite structure.

Chapter 4: Back coating of a ZnO substrate by sputtering

Both the side wall and the bottom surface of the ZnO substrate were also covered with a SiO_2 film followed by an AlN film. Both films were formed by using the sputtering system. A directly sputtered AlN film on the ZnO substrate appeared hexagonal domain features. It was partially exfoliated during annealing at 800 °C. Pits and hexagonal structures disappeared when both the thicknesses of AlN and SiO_2 were 800 nm.

Chapter 5: Growth of InGaN on ZnO by MOVPE with AlN protection layer

500-nm-thick InGaN films were grown on the ZnO substrates with the protection layers by MOVPE. For comparison, the MOVPE growth was also performed on both substrates of bare ZnO and sapphire. The InGaN film on the bare ZnO substrate exfoliated and the ZnO substrate was partially decomposed during the MOVPE growth. The decomposition of the ZnO substrate was suppressed with the protection layers. The MOVPE growth of the InGaN films were performed at various growth temperatures of 750 – 850 °C. The surface morphology of the InGaN film grown at 800 °C was relatively flat. The $In_{0.18}Ga_{0.82}N$ film on the ZnO substrate was almost unstrained.

6.2 Future work

In this thesis, the growth of the InGaN films on the ZnO substrates was achieved by MOVPE even though ZnO is not resistant to the H_2 atmosphere. This result has opened up the realm of the possibility for the growth of III-nitride semiconductors on the ZnO substrates. But, the research of the improvement and optimization will continue to be carried out with no more worries about the decomposition of the ZnO.

The higher efficiency of the LED at the longer wavelength can be expected by changing the materials of the protection layer. Recently, it is reported the growth of InGaN was demonstrated by pulsed sputtering deposition [78]. Therefore, the lattice matched protection layer will be utilized to improve the MOVPE-grown InGaN layer.

Reference

[1] T. Matsuoka, H. Tanaka, T. Sasaki, and A. Katsui, Inst. Phys. Conf. Ser., **106** (1990) 141.

[2] T. Matsuoka, H. Okamoto, M. Nakao, H. Harima, and E. Kurimoto, Appl. Phys. Lett., **81** (2002) 1246.

[3] S. Guha, J. M. DePuydt, J. Qiu, G. E. Hofler, M. A. Haase, B. J. Wu, and H. Cheng, Appl. Phys. Lett., **63** (1993) 3203.

[4] R. Haitz and J. Y. Tsao, Phys. Status Solidi A, **208** (2011) 17.

[5] M. R. Krames, O. B. Shchekin, R. Mueller-Mach, G. O. Mueller, L. Zhou, G. Harbers, and M. G. Craford, J. Display Technol., **3** (2007) 160.

[6] J. Hwang, R. Hashimoto, S. Saito, and S. Nunoue, Appl. Phys. Express, **7** (2014) 071003.

[7] S. Saito, R. Hashimoto, J. Hwang, and S. Nunoue, Appl. Phys. Express, **6** (2013) 111004.

[8] Y. Narukawa, M. Ichikawa, D. Sanga, M. Sano, and T. Mukai, J. Phys. D: Appl. Phys., **43** (2010) 354002.

[9] T. Sasaki and T. Matsuoka, J. Appl. Phys., **64** (1998) 4531.

[10] P. Kung, A. Slaxer, X. Zhang, D. Walker, R. Lavado, and M. Razeghi, Appl. Phys. Lett., **69** (1996) 2116.

[11] S. Nakamura, M. Senoh, S. Nagahama, N. Iwasa, T. Yamada, T. Masushita, H. Kiyoku, and Y. Sugimoto, Appl. Phys. Lett., **68** (1996) 2105.

[12] S. Chichibu, T. Azuhata, T. Sota, and S. Nakamura, Appl. Phys. Lett., **69** (1996) 4188.

[13] J. Yoo, S. Choi, S. Jung, Y. Cho, J. Lee, S. Lee, W. Lee, H. Lee, S. Kim, and J. Chang, J. Cryst. Growth, **370** (2013) 92.

[14] K. Ueno, A. Kobayashi, J. Ohta, and H. Fujioka, Appl. Phys. Lett., **90** (2007) 141908.

[15] E. M. Kaidashev, M. Lorenz, H. von Wenckstern, A. Rahm, H. C. Semmlhack, K. H. Han, G. Benndorf, C. Bundesmann, H. Hochmuth, and M. Grundmann, Appl. Phys. Lett., **82** (2003) 3901.

[16] T. Katase, H. Hiramatsu, H. Yanagi, T. Kamiya, M. Hirano, and H. Hosono, Solid State Commun., **149** (2009) 2121.

[17] A. Kuoni, R. Holzherr, M. Boillat, and N. F de Rooij, J. Micromech. Microeng. **13** (2003) S103.

[18] P. Tien, R. Ulrich, and R. Martin, Appl. Phys. Lett., **17** (1970) 447.

[19] C. Tsai, B. Sun, and A. Kar-Roy, Appl. Phys. Lett., **70** (1997) 3185.

[20] S. Shishiyanu, T. Shishiyanu, and O. Lupan, Sens. Actuators B, **107** (2005) 379.

[21] B. Pawar, G. Cai, D. Ham, R. Mane, T. Ganesh, A. Ghule, R. Shama, K. Jadhava, and S. Han, Sol. Energy Mater. Sol. Cells., **93** (2009) 524.

[22] R. Triboulet, Proc. SPIE, **4412** (2000) 1.

[23] C. R. Gorla, N. W. Emanetoglu, S. Liang, W. E. Mayo, Y. Lu, M. Wraback, and H. Shen, J. Appl. Phys., **85** (1999) 2595.

[24] K. Oka, H. Shibata, and S. Kashiwaya, J. Cryst. Growth, **237** (2002) 509.

[25] J. Nielsen and E. Dearborn, J. Phys. Chem., **64** (1960) 1762.

[26] X. Li, J. Xu, M. Jin, H. Shen, and X. Li, Chin. Phys. Lett., **23** (2006) 3356.

[27] D. Reynolds, C. Litton, D. Look, J. Hoelscher, B. Claflin, T. Collins, C. Nause, and B. Nemeth, J. Appl. Phys., **95** (2004) 4802.

[28] K. Oka, H. Shibata, and S. Kashiwaya, J. Cryst. Growth, **237** (2002) 5.

[29] D.C. Look, D. C. Reynolds, J. R. Sizelove, R. L. Jones, C. W. Litton, G. Cantwell, and W. C. Harsch, Solid State Commun., **105** (1998) 399.

[30] N. Sakagami and K. Shibayama, Jpn. J. Appl. Phys., **20** (1981) 201.

[31] D. Ehrentraut, K. Maeda, M. Kano, K. Fujii, and T. Fukuda, J. Cryst. Growth, **320** (2011) 18.

[32] M. J. Callahan, D. Ehrentraut, M.N. Alexander, and B. Wang, "Zinc Oxide Materials for Electronic and Optoelectronic Device Applications," Wiley, C. W. Litton, T. C. Collins, D. C. Reynolds (Eds.), pp. 189-194, 2011.

[33] E. Ohshima, H. Ogino, I. Niikura, K. Maeda, M. Sato, M. Ito, and T. Fukuda, J. Cryst. Growth, **260** (2004) 166.

[34] H. Ko, M. Han, Y. Park, Y. Yu, B. Kim, S. Kim, and J. Kim, J. Cryst. Growth, **269** (2004) 493.

[35] S. Graubner, C. Neumann, N. Volbers, B. K. Meyer, J. Blasing, and A. Krost, Appl. Phys. Lett., **90** (2007) 042103.

[36] A. Kobayashi J. Ohta, and H Fujioka, Jpn. J. Appl. Phys., **45** (2006) 5724.

[37] X. Gu, S. Sabuktagin, A. Teke, D. Johnstone, H. Morkoç, B. Nemeth, and J. Nause, J. Mater. Sci. Mater. Electron., **15** (2004) 373.

[38] L. S. Vlasenko and G. D. Watkins, Phys. Rev. B, **71** (2005) 125210.

[39] H. M. Christen, D. P. Norton, L. A. Gea, and L. A. Boatner, Thin Solid Films, **312** (1998) 156.

[40] H. N. Lee, H. M. Christen, M. F. Chisholm, C. M. Rouleau, and D. H. Lowndes, Nature, **433** (2005) 395.

[41] H. Yamada, M. Kawasaki, Y. Ogawa, and Y. Tokura, Appl. Phys. Lett., **81** (2002) 4793.

[42] D. G. Schlom, J. H. Haeni, J. Lettieri, C. D. Theis, W. Tan, J. C. Jiang, and X. Q. Pan, Mater. Sci. & Eng. B, **87** (2001) 282.

[43] M. P. Warusawithana, E. V. Colla, J. N. Eckstein, and M. B. Weissman, Phys. Rev. Lett., **90** (2003) 1586.

[44] E. S. Hellman, D. N. E. Buchanan, D. Wiesmann, and I. Brener, MRS Intern. J. Nitride Semicond. Res., **1** (1996) 1.

[45] T. Suzuki, C. Harada, H. Goto, T. Minegishi, A. Setiawan, H. J. Ko, M. W. Cho, and T. Yao, Curr. Appl. Phys., **4** (2004) 643.

[46] G. Namkoong, S. Burnham, K. Lee, E. Trybus, W. A. Doolittle, M. Losurdo, P. Capezzuto, G. Bruno, B. Nemeth, and J. Nause, Appl. Phys. Lett., **87** (2005) 184104.

[47] C. Chang, H. Huang, Y. Lan, T. Lu, L. Tu, and W. Hsieh, Crys. Growth Des., **13** (2013) 3098.

[48] K. Ueno, A. Kobayashi, J. Ohta, H. Amanai, S. Nagao, H. Horie, and H. Fujioka, Appl. Phys. Lett., **91** (2007) 08915.

[49] T. Kajima, A. Kobayashi, K. Shimomoto, K. Ueno, T. Fujii, J. Ohta, H. Fujioka, and M. Oshima, Phys. Status Solidi RRL, **5** (2011) 400.

[50] J. F. Muth, R. M. Kolbas, A. K. Sharma, S. Oktyabrsky, and J. Narayan, J. Appl. Phys. **85** (1999) 7884.

[51] K. Okamoto, S. Inoue, N. Matsuki, T. W. Kim, H. Fujioka, and M. Oshima, Phys. Status Solidi A, **202** (2005) R149.

[52] Z. Toth, B. Hopp, T. Smausz, Z. Kantor, F. Ignacz, T. Szorenyi, and Z. Bor, Appl. Surf. Sci., **138-139** (1999) 130.

[53] G. A. Slack and T. F. McNelly, J. Cryst. Growth, **34** (1987) 263.

[54] R. M. German, “Sintering Theory and Practice,” Wiley, New York, pp. 1-13, 1996.

[55] S. Hampshire, “Sintering of Nitrogen Ceramics,” The Parthenon press, Carnforth, pp. 47-52, 1986.

[56] P. Vennéguès, B. Beaumont, S. Haffouz, M. Vaille, and P. Gibart, J. Cryst. Growth, **187** (1998) 167.

[57] D. W. Hoffman and J. A. Thornton, Thin Solid Films, **45** (1977) 387.

[58] H. Y. Liu, G. S. Tang, F. Zeng, and F. Pan, J. Cryst. Growth, **363** (2013) 80.

[59] H. Iwanaga, A. Kunishige, and S. Takeuchi, J. Mater. Sci., **35** (2000) 2451.

[60] J. B. Wachtman, T. G. Scuderi, and G. W. Cleek, J. Am. Ceram. Soc., **45** (1962) 319.

[61] S. Ruvimov, Z. Liliental-Weber, T. Suski, J. W. Ager III, J. Washburn, J. Krueger, C. Kisielowski, E. R. Weber, H. Amano, and I. Akasaki, Appl. Phys. Lett., **69** (1996) 990.

[62] I. Lee, I. Choi, C. Lee, E. Shin, D. Kim, S. K. Noh, S. Son, K. Lim, and H. J. Lee, J. Appl. Phys., **83** (1998) 5787.

[63] L. T. Romano, C. G. Van de Walle, J. W. Ager III, W. Gtz, and R. S. Kern, J. Appl. Phys., **87** (2000) 7745.

[64] C. G. Van de Walle, Phys. Rev. B, **68** (2003) 165209.

[65] A. Costales, M. A. Blanco, A. M. Pendas, A. K. Kandalam, and R. Pandey, J. Am. Chem. Soc., **124** (2002) 4116.

[66] N. Li, S. Wang, C. Huang, Z. Feng, A. Valencia, J. Nause, C. Summers, and I. Ferguson, J. Cryst. Growth, **310** (2008) 4908.

[67] Y. Lei, J. Xu, K. Zhu, M. He, J. Zhou, Y. Gao, L. Zhang, and Y. Chen, J. Display Tech., **9** (2013) 377.

[68] Y. Izawa, T. Oga, T. Ida, K. Kuriyama, A. Hashimoto, H. Kotake, and T. Kamijoh, Appl. Phys. Lett., **99** (2011) 021909.

[69] A. R. A. Zauner, E. Aret, W. J. P. van Enckevort, J. L. Weyher, S. Porowski, and J. J. Schermer, J. Cryst. Growth **240** (2002) 14.

[70] S. Keller, N. A. Fitenbaum, F. Wu, D. Brown, A. Rosales, S. P. DenBaars, J. S. Speck, and U. K. Mishra, J. Appl. Phys., **102** (2007) 083546.

[71] Q. Sun, Y. Cho, B. Kong, H. Cho, T. Ko, C. D. Yerino, I. Lee, and J. Han, J. Cryst. Growth, **311** (2009) 2948.

[72] T. Matsuoka, N. Yoshimoto, T. Sasaki, and A. Katsui, J. Electronic Mat., **21** (1992) 157.

[73] N. Li, S. Wang, C. Huang, Z. Feng, A. Valencia, J. Nause, C. Summers, and I. Ferguson, J. Cryst. Growth, **310** (2008) 4908.

[74] Y. Lei, J. Xu, K. Zhu, M. He, J. Zhou, Y. Gao, L. Zhang, and Y Chen, J. Display Tech., **9** (2013) 377.

[75] S. Wang, N. Li, E. Park, S. Lien, Z. Feng, A. Valencia, J. Nause, and I. Ferguson, J. Appl. Phys., **102** (2007) 106105.

[76] Y. Kawai, S. Ohtsuka, M. Iwaya, S. Kamiyama, H. Amano, and I. Akasaki, J. Cryst. Growth, **311** (2009) 2929.

[77] Y. Kawai, S. Ohsuka, M. Iwaya, S. Kamiyama, H. Amano, and I. Akasaki, Phys. Status Solidi C, **9** (2008) 3023.

[78] A. Kobayashi, J. Ohta, and H. Fujioka, Nature Sci. Rep., **7** (2017) 12820.

Achievements

Publication

1. Jinyeop Yoo, Shojiki Kanako, Tomoyuki Tanikawa, Shigeyuki Kuboya, Takashi Hanada, Ryuji Katayama, and Takashi Matsuoka, "Polarity control of MOVPE grown GaN on AlN/GaN templates," Jpn. J. Appl. Phys., **55** (2016) 05FA041.

Presentations

1. J. Yoo, J. Chang, J. Lee, S. Choi, S. Lee, H. Lee, S. Kim, and T. Matsuoka, "Reduction of impurity out-diffusion during HVPE growth of GaN on ZnO by using $ZnAl_2O_4$ interlayer," ISAC-5 in conjunction with ASPT2013, D10-13 (Wuhan, China, 13, Dec., 2013).
2. J. Yoo, J. Chang, J. Lee, S. Choi, H. Lee, S. Kim, T. Tanikawa, R. Katayama, and T. Matsuoka, "$ZnAl_2O_4$ Interlayer for Suppressing Impurity Out-diffusion in HVPE Growth of GaN on ZnO Substrate," The 33rd Electronic Materials Symposium, Th 3-3 (Shizuoka, Japan, 10, Jul., 2014).
3. J. Yoo, J. Chang, H. Lee, S. Kim, and T. Matsuoka, "$ZnAl_2O_4$ Interlayer for Suppressing Impurity Out-diffusion in HVPE Growth of GaN on ZnO Substrate," The 128th IMR Lecture Meeting, P5 (Sendai, Japan, 27, Nov., 2014).
4. J. Yoo, K. Shojiki, T. Tanikawa, S. Kuboya, T. Hanada, R. Katayama, and T. Matsuoka, "MOVPE growth of GaN onto PLD-grown AlN interlayer on GaN templates," LEDp2-5 (Yokohama, Japan, 23, Apr., 2015).
5. J. Yoo, K. Shojiki, T. Tanikawa, S. Kuboya, T. Hanada, R. Katayama, and T. Matsuoka, "Polarity control of MOVPE grown GaN on AlN/GaN templates," Nano Structure・Epitaxial Growth Workshop, 2015 Spring Lecture Meeting, Fr-04 (Sendai, Japan, 8, May, 2015).
6. J. Yoo, K. Shojiki, T. Tanikawa, S. Kuboya, T. Hanada, R. Katayama, and T. Matsuoka, "Polarity control of GaN growth on PLD-AlN/GaN templates by MOVPE," The 129th IMR Lecture Meeting, P81 (Sendai, Japan, 29, May, 2015).
7. J. Yoo, K. Shojiki, T. Tanikawa, S. Kuboya, T. Hanada, R. Katayama, and T. Matsuoka, "Polarity-controlled MOVPE growth of GaN on PLD-AlN template", The 34th Electronic Materials Symposium, We 1-11 (Shiga, Japan, 15, Jul., 2015).

8. Y. Mitani, R. Katayama, J. Yoo, K. Shojiki, T. Tanikawa, S. Kuboya, and T. Matsuoka, “Design of the Transverse Quasi Phase Matched AlN Waveguides for Deep-UV Second Harmonic Generation,” The 34th Electronic Materials Symposium, We 1-12 (Shiga, Japan, 15, Jul., 2015).
9. J. Yoo, K. Shojiki, T. Tanikawa, S. Kuboya, T. Hanada, R. Katayama, and T. Matsuoka, “Polarity control of GaN grown on PLD-AlN/GaN templates by MOVPE,” The 6th International Symposium on Growth of III-Nitrides, TuA-3 (Hamamatsu, Japan, 10, Nov., 2015).
10. J. Yoo, R. Katayama, S. Kuboya, T. Tanikawa, T. Hanada, and T. Matsuoka, “Growth of InGaN films on ZnO substrates via AlN protection layers by metalorganic vapor phase epitaxy,” The 133rd IMR Lecture Meeting, P28 (Sendai, Japan, 26, May, 2017).
11. J. Yoo, T. Tanikawa, S. Kuboya, T. Hanada, R. Katayama, K. Omura, and T. Matsuoka, “Comparison of the InGaN growth on bare ZnO substrate and AlN/ZnO template by metalorganic vapor phase epitaxy,” The 135th IMR Lecture Meeting, P72 (Sendai, Japan, 23, May, 2018)

Award

1. 2016 Japan-Russia joint seminar & 2015 Annual meeting of excellent graduate schools, Poster presentation award, (Mar, 2016).